


A Conserved Mito-Cytosolic Translational Balance Links Two Longevity Pathways

Journal Article

Author(s):

Molenaars, Marte; Janssens, Georges E.; Williams, Evan Graehl ; Jongejan, Aldo; Lan, Jiayi; Rabot, Sylvie; Joly, Fatima; Moerland, Perry D.; Schomakers, Bauke V.; Lezzerini, Marco; Liu, Yasmine J.; McCormick, Mark A.; Kennedy, Brian K.; van Weeghel, Michel; van Kampen, Antoine H.C.; Aebersold, Ruedi; MacInnes, Alyson W.; Houtkooper, Riekelt H.

Publication date:

2020-03-03

Permanent link:

<https://doi.org/10.3929/ethz-b-000403809>

Rights / license:

[In Copyright - Non-Commercial Use Permitted](#)

Originally published in:

Cell Metabolism 31(3), <https://doi.org/10.1016/j.cmet.2020.01.011>

Funding acknowledgement:

670821 - Proteomics 4D: The proteome in context (EC)

A conserved mito-cytoplasmic translational balance links two longevity pathways

Marte Molenaars^{1*}, Georges E. Janssens^{1*}, Evan G. Williams², Aldo Jongejan³, Jiayi Lan²,
Sylvie Rabot⁴, Fatima Joly⁴, Perry D. Moerland³, Antoine H.C. van Kampen³, Ruedi
Aebersold^{2,5}, Alyson W. MacInnes¹, Riekelt H. Houtkooper^{1,6#}

¹Laboratory Genetic Metabolic Diseases, Amsterdam UMC, University of Amsterdam, Meibergdreef 9,
Amsterdam, The Netherlands

²Institute of Molecular Systems Biology, ETH Zurich, 8093 Zürich, Switzerland

³Bioinformatics Laboratory, Amsterdam UMC, University of Amsterdam, Meibergdreef 9, Amsterdam, The
Netherlands

⁴Micalis Institute, INRA, AgroParisTech, Université Paris-Saclay, Jouy-en-Josas, France

⁵Faculty of Science, University of Zürich, Switzerland

⁶Lead contact

* Equal contributions

#Correspondence: r.h.houtkooper@amc.nl (RHH)

Summary

Slowing down mRNA translation in either the cytoplasm or the mitochondria are conserved longevity mechanisms. Here, we found a non-interventional natural correlation of mitochondrial and cytoplasmic ribosomal proteins (RPs) in mouse population genetics, suggesting a translational balance between these two compartments. Inhibiting mitochondrial translation in *C. elegans* through *mrps-5* RNAi repressed overall cytoplasmic translation. Transcriptomics integrated with proteomics revealed that this inhibition specifically reduced the translational efficiency (TE) of mRNAs required in growth pathways while increasing the TE of stress response mRNAs. The coordinated repression of cytoplasmic translation is dependent on *atf-5/Atf4* and is conserved in mammalian cells upon inhibiting mitochondrial translation pharmacologically with the antibiotic doxycycline. Lastly, extending this *in vivo*, doxycycline repressed cytoplasmic translation and RP expression in the livers of germ-free mice. These data demonstrate that inhibiting mitochondrial translation initiates an *atf-5/Atf4*-dependent cascade leading to coordinated repression of cytoplasmic translation, which could be targeted to promote longevity.

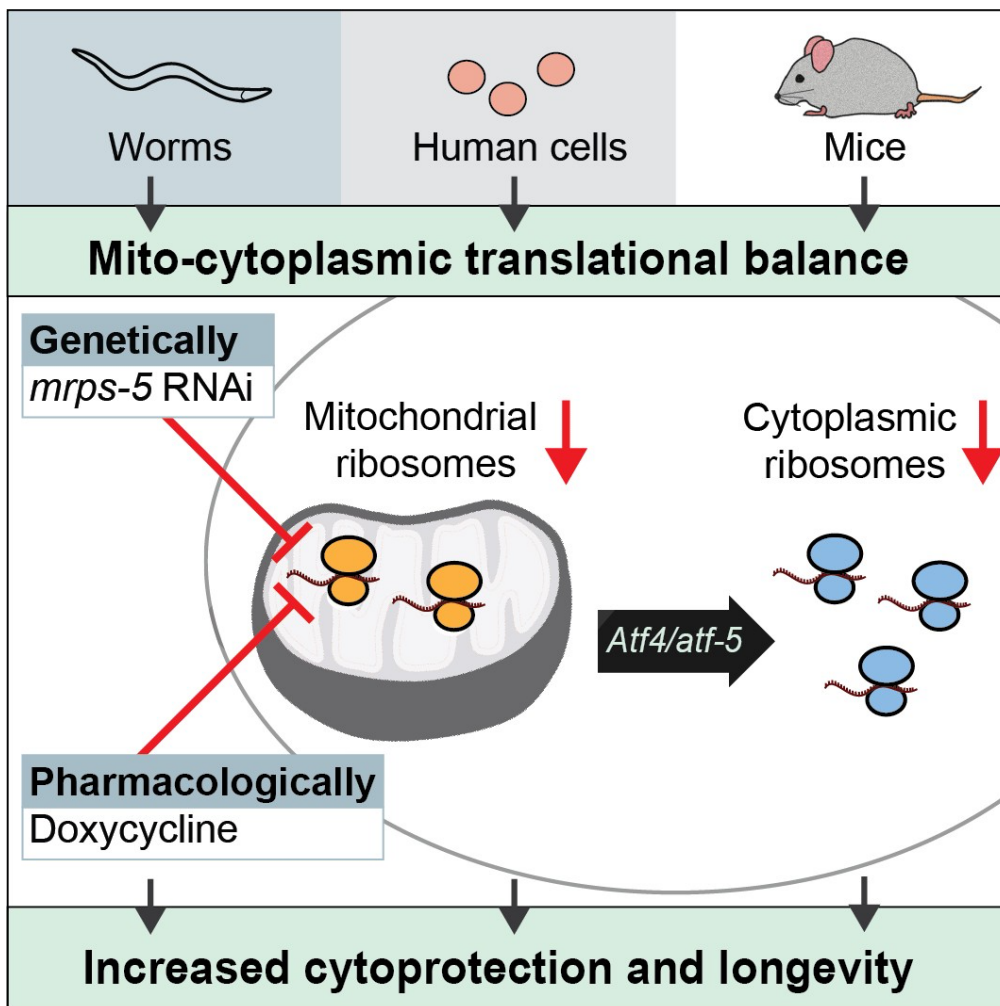
Keywords

longevity / ribosomes / mitochondrial translation / cytoplasmic translation / translational balance

Highlights

- Mitochondrial and cytoplasmic RP levels balance in a natural stoichiometric ratio
- Blocking mitochondrial ribosomes in worms and mice reduces cytoplasmic translation
- This translational balance is ATF4/*atf-5* dependent and conserved in human cells
- Translational efficiency of RP transcripts changes in response to ratio requirement

Graphical abstract



Introduction

The translation of mRNA into protein is essential for the growth and survival of every cell. Translation is carried out by small and large ribosomal subunits associating with mRNA assisted by eukaryotic initiation factors (eIFs) and elongation factors (eEFs) to ensure its speed and accuracy. The biogenesis of ribosomes coupled to mRNA translation has been estimated to be the most energy-consuming process in the cell (Buttgereit and Brand, 1995; Lane and Martin, 2010; Wieser and Krumschnabel, 2001). Slowing down translation by reducing expression of ribosomal proteins (RPs), eIFs/eEFs, or ribosomal RNA (rRNA) results in lifespan extension in yeast, worms, and flies (Chiocchetti et al., 2007; Hansen et al., 2007; Pan et al., 2007). This suggests a universal mechanism of lifespan extension lies in conserving the energy normally expended on cytoplasmic mRNA translation.

Distinct from the ribosomes in the cytoplasm, ribosomes reside in the mitochondria that are dedicated to translating the mRNAs encoded by the mitochondrial DNA. Due to the endosymbiotic 'bacterial' origin of the mitochondria, mitochondrial ribosomes are structurally more similar to bacterial ribosomes than to their cytoplasmic counterparts (Greber et al., 2015; Greber et al., 2014; Smits et al., 2007). Compared to cytoplasmic ribosomes, mitochondrial ribosomes only need to translate a relatively small set of 13 mRNAs coding for subunits of the oxidative phosphorylation (OXPHOS) complexes that are required for the generation of ATP. Remarkably, slowing down mitochondrial translation also extends lifespan (Houtkooper et al., 2013). Inhibiting mitochondrial translation genetically (e.g. by knocking down mitochondrial ribosomal genes) or pharmacologically (e.g. by using the antibiotic doxycycline) results in mitonuclear protein imbalance and activates the mitochondrial unfolded protein response (UPR^{mt}) in a process conserved from worms to mammals (Houtkooper et al., 2013; Jovaisaite and Auwerx, 2015). The UPR^{mt} includes the upregulated expression of cytoprotective genes, such as those coding for mitochondrial heat shock proteins 6 and 60 (*hsp-6 and hsp-60*) (Haynes and Ron, 2010). Other

aspects of this response initiated by stressed mitochondria are mediated by *Atf4* (*C. elegans atf-5*) (Quiros et al., 2017), a cyclic AMP-dependent transcription factor that has been implicated in a variety of mouse longevity models (Li et al., 2014).

Although mitochondrial and cytoplasmic ribosomes are separate translational apparatuses they depend on each other to coordinate mitochondrial function, in particular the synthesis of OXPHOS proteins. A regulatory signaling route from cytoplasmic translation to mitochondrial translation has been reported in yeast, which allegedly is strictly unidirectional (Couvillion et al., 2016). However, since mitochondria produce cellular energy and translation in the cytosol is a vast consumer of this energy, we hypothesized that there may be bidirectional translational control.

Here, we investigated the correlation of abundances between mitochondrial and cytoplasmic RPs in the BXD genetic reference population of mice (Wang et al., 2016). To address the direct link between mitochondrial and cytoplasmic translation, we have used a worm model of genetically impaired mitochondrial translation (RNAi mediated knockdown of *mrps-5*) and observed a decrease in cytoplasmic translation using polysome profiling. By integrating 'omics' data on three levels of biology [transcriptomics of the whole worm, transcriptomics of the polysomal fraction of the worm (highly translated transcripts), and proteomics], we explored an integrated, system-level view of the molecular changes induced via knockdown of mitochondrial translation that result in longevity. To show that key elements of this process are evolutionarily conserved, we used the antibiotic doxycycline as a means to reduce mitochondrial translation in human K562 cells and *in vivo* in mice. The findings of this study indicate a bidirectional regulation exists between the two translation machineries across species, regulating longevity.

Results

Mitochondrial and cytoplasmic ribosomal proteins co-correlate in a natural population of mice

The degree to which the mitochondrial and cytoplasmic ribosomes longevity pathways regulate one another is not well understood (illustrated in Figure 1A). However, it seems likely that cross-communication between these systems exists allowing for the suppression of translation should either machinery become compromised in order to maintain equal rates of production. Therefore, one would expect the natural abundances of these two translation machineries to match one another in varying cell types, tissues, or individuals in a population. In order to evaluate the possible natural balance in abundances that occurs between elements of the mitochondrial and cytoplasmic translational machinery, we turned to the population of BXD mouse strains. These segregate for around 5 million sequence variants, which in turn lead to expression variation in the transcriptome and proteome with a complexity similar to human populations (Wang et al., 2016). To resolve the relationships between the mitochondrial and cytoplasmic translation machineries in the mouse BXD liver proteome data, we reconstructed the protein correlation network between the individual elements of these protein complexes (Figure 1B, Table S1). Using a fairly permissive cutoff criteria ($p < 5e-4$), we observed robust correlations both within the subunits of the cytoribosome and mitoribosome ($p < 1e-4$, $p = 0.014$, respectively), and importantly, strong interactions *between* these translation machineries ($p < 1e-4$). To confirm the robustness of this observation, we turned to a separate mouse study (Williams et al., 2018) examining the regulation of proteins across eight BXD strains and across four different tissues (Figure 1B). Indeed, we found RPs from both ribosome types clustered and co-varied as observed in the liver-specific data, suggesting a general mechanism is in place ensuring mito-cytoplasmic translational balance. As expected, taking the average abundance of either cytoplasmic or mitochondrial RPs for each BXD strain showed variation to exist within each ribosome type (Figure 1C), and evaluating average mitochondrial ribosome abundances in relation to the average levels of cytoplasmic

ribosomes within individual BXD strains, confirmed the strong correlation between these two translation machineries (Pearson $R = 0.60$, $p < 0.05$) (Figure 1D). Taken together, these findings demonstrate that mitochondrial ribosome and cytoplasmic ribosome abundances are tightly regulated to stay in natural stoichiometric ratios.

Previous work in yeast has suggested a unidirectional relationship between these two translation machineries, where disruption of cytoplasmic ribosomes can concomitantly reduce abundances of mitochondrial ribosomes but not the reverse (Couvillion et al., 2016). To test the hypothesis that regulation could also occur in the opposite direction, namely mitochondrial ribosomes influencing the cytoplasmic ribosomes, we turned to *C. elegans* with reduced levels of mitochondrial small ribosomal protein 5 (*mrps-5*). In addition to inhibiting mitochondrial translation, RNAi of *mrps-5* induces the mitochondrial unfolded protein response (UPR^{mt}), alters mitochondrial function, prevents aging-associated functional decline, and extends lifespan in *C. elegans* (Houtkooper et al., 2013). To assess the status of cytoplasmic translation in *mrps-5* worms, we used a polysome profiling technique where free ribosomal subunits, monosomes (mRNA with one ribosome associated), and polysomes (mRNA with two or more ribosomes associated), are separated over a sucrose density gradient and quantified by optical density. Remarkably, in *mrps-5* RNAi treated worms we observed a shift from polysomes to monosomes, suggesting that more cytoplasmic mRNAs are being translated by a single ribosome instead of multiple following mitochondrial translation inhibition (Figure 1E). Indeed, quantification of the profiles confirmed a significant reduction of polysomal peaks in the *mrps-5* worms, revealing a suppression of cytoplasmic translation occurring in worms with an impaired mitochondrial ribosome (Figure 1F). This observation establishes that in addition to the established communication from the cytoplasm and mitochondria, a second and novel relationship exists whereby the mitochondrial ribosome communicates with the cytoplasmic translational machinery.

***mrps-5* RNAi treated worms display reduced translational efficiency (TE) of cytoplasmic ribosomal proteins**

Having observed a decrease in global translation occurring in *mrps-5* RNAi treated worms, we next inquired as to what genes are specifically repressed at the translational level, i.e. in our polysomal fractions. In order to do so, we generated RNA-seq libraries of polysomal and monosomal fractions of RNA from *mrps-5* and control worms for comparison. The RNA-seq transcriptomes provided reliable quantification of over 16000 genes covering the majority of the worm genome, allowing for a global description of the differences existing between monosome and polysomal RNA fractions (Figure 2A, Table S2).

To capture the broad-spectrum set of changes that discriminate between *mrps-5* and control worms at either the monosomal or polysomal levels, we performed a partial least squares discriminant analysis (PLS-DA) on the samples for each condition. We found this to effectively distinguish *mrps-5* from control worms (Figure 2B-C, Table S2). Notably, this method is effective as a feature selector in addition to a sample classifier and is therefore useful in that it provides a variable of importance (VIP) ranking for each gene corresponding to its contribution in group discrimination (Boulesteix and Strimmer, 2007). This VIP score correlates highly to traditional *p*-value ranking (Figure S1A-B), though allows for a broader set of changes to be considered, which is more representative of the multifactorial nature of complex biological phenotypes. To explore the biological differences between groups in this way, we assessed genes with a high VIP score (>1) and turned to the DAVID bioinformatics resource (Huang da et al., 2009). DAVID analysis clusters enrichments in Gene Ontologies (GO) and various pathway databases, including KEGG and Interprot, based on recurrence and similarities of genes in enriched pathways. With this method we noted a wide variety of changes between *mrps-5* RNAi and control worms (Table S2). For instance, changes in the *mrps-5* monosomal RNA included an upregulation of RNAs coding for mitochondrial transit peptides (e.g. genes *asg-2*, *atad-3*, *cyc-2.1*) and a suppression of RNAs

important for cuticle formation and other developmental pathways (e.g. genes *bli-6*, *col-81*, *rol-1*). A parallel upregulation of RNAs coding for mitochondrial transit peptides in the polysomes of *mrps-5* (i.e. genes *aco-2*, *coq-8*, *phb-2*) was also found along with a similar suppression of RNAs coding for proteins important for reproduction and growth (e.g. genes *acn-1*, *epi-1*, *ptr-4*) (Table S2).

In order to identify what transcripts were shifting from polysomal to monosomal fractions, and vice versa, we calculated the translational efficiency (TE) of each gene. The TE is defined as the ratio of the polysomal RNA to the monosomal RNA fraction, for *mrps-5* RNAi relative to control worm. Upon log₂ transformation, a positive TE value then corresponds to transcripts that shift from the monosome to the polysome in *mrps-5* RNAi relative to control, while negative TE values correspond to a shift in the opposite direction (Figure 2D, Table S2). Setting a low minimal fold change TE cutoff of 1.25 with a significant VIP score in at least one of the two group comparisons, we assessed genes with altered TE using DAVID GO term clustering. This analysis revealed that upon *mrps-5* RNAi, genes with a high TE were coding for membrane components, proteins involved in stabilization of membrane potential, and proteins used in oxygen transport that include genes such as *aat-7*, *dpy-19*, and *rom-5* (Figure 2E-F, Table S2). This observation is likely reflecting the worm's need to adapt to its altered mitochondrial biology. Strikingly, genes with a low TE were by and large coding for proteins involved in translation and ribosome biogenesis (Figure 2E, Table S2), suggesting that *mrps-5* RNAi worms suppress the translation of cytoplasmic ribosome components. These genes included translation elongation factors such as *eif-3.B*, *eif-3.C*, and *eif-3.D* (Figure 2F), in addition to those coding for the vast majority of RPs. Remarkably, visualizing the TE of the ribosome-associated proteins individually highlights what amounts to be almost a complete repression of the genes coding for the RPs that assemble the cytoplasmic ribosome (Figure 2G). These findings demonstrate the *mrps-5*-deficient mitochondrial translation machinery wields a strong regulatory influence over the cytoplasmic ribosomal translation machinery.

***mrps-5* worms suppress growth pathways and upregulate stress responses at both the proteome and transcriptome levels**

To better understand how the transcriptional responses ensuing from *mrps-5* RNAi impact the proteome, we next performed both whole worm RNA-seq, and SWATH mass spectrometry proteomics of *mrps-5* RNAi versus empty vector control worms. Our whole worm RNA profiling tracked the abundances of over 16000 transcripts (Table S3), while proteomics was able to quantify over 1700 proteins (Table S4). Again, the worm samples were readily distinguished through PLS-DA (Figure 3A-C), attributable to the large differences inherent between *mrps-5* RNAi worms and controls reflected at both the transcript and protein levels. Using the VIP scores from the PLS-DA classification, we found major changes in the *mrps-5* RNAi worms. These are characterized by an upregulation of oxidation-reduction and glycolysis-related genes and a downregulation of development, growth, and reproduction-related genes at the transcript level (Table S3). At the protein level we found an upregulation of mitochondrial (transit peptides) and nucleosome assembly proteins and a downregulation of the mitochondrial respiratory chain (complex I) subunits along with proteins involved in development and reproduction (Table S4).

To better understand if the changes detected at the transcript and protein levels were representative of one another, we assessed the 1407 protein-transcript pairs overlapping between both 'omics' datasets (Table S5). Given their good correlation in abundance (Figure 3D-E), we proceeded to check their differences in a co-regulation analysis. This was achieved by investigating fold changes occurring at the transcript level versus those occurring at the protein level for each individual gene and protein (Figure 3F). To reduce noise, we omitted genes with near zero-fold changes (those within dashed lines in Figure 3F) and again used the PLS-DA derived (Figure 3B-C) VIP scores for selection criteria, whereby a VIP score >1 identified genes contributing to the difference between control and *mrps-5* RNAi treated worms. Our co-regulation analysis showed that the majority (67%) of genes were similarly regulated at the protein and

transcript levels in *mrps-5* RNAi worms (Figure 3F, pie chart inset and scatterplot, whereby 36% were co-upregulated [Q1] and 31% were co-downregulated [Q3]). Manual inspection of co-upregulated (Q1) genes revealed an increase antioxidant-related defense genes such as *sod-1*, *coq-3*, and *coq-6* as well as the UPR^{mt} proteins *hsp-6* and *hsp-60*, the latter of which are in line with what we previously reported (Houtkooper et al., 2013). Co-downregulated genes (Q3) included growth- and translation-related genes such as *eif-3.E*, *eif-3.G*, *rpl-11.1* and *rpl-25.2* (Figure 3G). While only a minority (9%) of genes were downregulated at the transcript level and upregulated at the proteins level (Q2), our co-regulation analysis demonstrated that a sizeable proportion of genes (24%) exhibited an upregulation at the transcript level and a downregulation at the protein level (Q4). Manual inspection showed these genes to be predominantly related to cellular respiration, such as the NADH:ubiquinone oxidoreductase core subunit genes *nduf-6*, *nduf-7*, *nuo-2*, *nuo-3*, *nuo-6* (Figure 3G). While the upregulation at mRNA level likely reflects the worm's need to adapt to a loss of respiratory capacity from *mrps-5* RNAi, the OXPHOS complexes cannot be assembled properly due to the lack of their mitochondrial translated partners and are downregulated on the protein level.

To better understand changes present in each quadrant of our co-regulation plot, we performed GO term enrichment analyses (Figure 3H-K, Table S5). While the genes associated with upregulated proteins and downregulated transcripts had relatively few enriched GO terms (Figure 3H), the remaining quadrants showed strong enrichments. Co-upregulated (Q1) genes enriched for mitochondrial-related processes likely reflecting an active adaptation in mitochondria to the knockdown of *mrps-5* (Figure 3I). Co-downregulated (Q3) gene enrichments supported a role for decreased growth and development, with such terms as “nematode larval development” and “structural constituent of cuticle,” being most prominent (Figure 3J). Meanwhile, as observed in the individual gene analysis, genes with upregulated transcripts and downregulated proteins showed enrichments for OXPHOS (Figure 3K). Taken together, co-suppression of the individual

translation-related genes in Q2 (Figure 3G) with the suppression of developmental related processes (Figure 3J) supports the idea that mitochondrial ribosomes crosstalk with cytoplasmic growth pathways to adapt the worm to a low energy state. Indeed, this adaptation is reflected in protein components of the worm's respiratory chain, whereby OXPHOS proteins were suppressed despite their transcriptional upregulation (Figure 3G, K).

The mitochondrial to cytoplasmic translation response is dependent on the *atf-5/Atf4* transcription factor and is conserved in mammalian cells

Our proteome-transcriptome co-regulation analysis of *mrps-5* RNAi worms indicates that the upregulation of cytoprotective genes and downregulation of growth and biogenesis-related genes is to a significant extent a transcriptionally-regulated phenotype. This suggests that transcription factors may be core mediators of this process. Recent studies identified the transcription factor *Atf4* (*atf-5* in *C. elegans*) as a key player in communication from mitochondria towards the cytosol during mitochondrial stress induced by inhibition of either mitochondrial import, OXPHOS, membrane potential, or mitochondrial translation (Quiros et al., 2017). Elevated levels of ATF4 were also observed in many mouse longevity models that involve the suppression of cytoplasmic translation (Li et al., 2014). Given these reports, we investigated a potential role of *C. elegans atf-5* coordinating the balance between cytoplasmic and mitochondrial translation. Using polysome profiling, we observed that the decreased cytoplasmic translation occurring in *mrps-5* RNAi worms is almost fully restored to control levels upon additional feeding of *atf-5* RNAi to worms (Figure 4A). Indeed, quantification of the peaks in the polysome profiles showed significant rescue of the repressed polysomal peaks in *mrps-5* worms when *atf-5* was also knocked down (Figure 4B). This epistasis experiment implicated *atf-5* as a mediator of the suppression of cytoplasmic translation that is induced by the suppression of mitochondrial translation via *mrps-5* knockdown.

In order to see if this communication between mitochondrial translation machinery and cytoplasmic translation machinery is conserved in mammalian cells, we turned to a pharmacological model of reducing mitochondrial translation with the antibiotic doxycycline. Doxycycline is in the tetracycline family of antibiotics that inhibits mitochondrial translation by binding the mitochondrial small ribosomal subunit, while in contrast other antibiotics such as amoxicillin target bacterial cell wall synthesis. Amoxicillin is used here as a control in line with our previous work (Houtkooper et al., 2013; Moullan et al., 2015) (Figure 4C). The human K562 leukemia cell line was treated with DMSO, amoxicillin, or doxycycline and subjected to polysome profiling. We found that doxycycline treatment resulted in an overall repression of all peaks, including the monosomal and polysomal fractions, revealing a global repression of cytoplasmic translation as a result of mitochondrial translation inhibition (Figure 4D). In line with our observations that the *C. elegans atf-5* is involved in this response, we observed that protein expression of ATF4, the mammalian homolog of *atf-5*, is upregulated in doxycycline- but not amoxicillin-treated K562 cells (Figure 4E). Taken together, these findings suggest that ATF4/*atf-5* is mediating the communication between mitochondrial and cytoplasmic translation machineries in a manner that is conserved from nematodes to mammals.

The mitochondrial to cytoplasmic translation response is conserved *in vivo* in mice

Having observed a conserved repression of cytoplasmic translation upon inhibition of mitochondrial translation in mammalian cells with doxycycline treatment, we next investigated these effects *in vivo* in mice. We treated mice for two weeks with doxycycline or amoxicillin in their drinking water, using doses that were previously reported to induce a mitonuclear protein imbalance (Moullan et al., 2015). To eliminate potential indirect effects of the antibiotics through the microbiome, we performed the antibiotic treatments on germ-free C57BL/6J mice. We found that doxycycline treatment resulted in suppression of global translation in liver in a dose-dependent manner (Figure S2). Following this, we performed RNA-seq of the polysomal and total RNAs of liver tissue harvested from the antibiotic-treated mice (Figure 5A, Table S6). Similar as

to what was observed in worms, we found the samples were readily classified through PLS-DA (Figure 5B-C) and again used VIP scores to distinguish differentially expressed genes (VIP > 1). DAVID analysis of the RNA-seq results showed a striking downregulation of translation-related genes in the polysomal RNA fractions of doxycycline-treated mice (Figure 5D, Table S6), and an upregulation of various cellular defense processes including oxidation-reduction (Figure 5E) that is in line with our observations in *mrps-5* deficient *C. elegans*. This suppression of cytoplasmic ribosomes was greater in the polysomal RNA fraction (Figure 5F) than in total RNA (Figure S3B), together resulting in a suppression of the TE of ribosomal genes occurring in doxycycline-treated mice (Figure S3A, S3C, Table S6). Mitochondrial ribosomes were most strongly suppressed at the total RNA level (Figure S3D-E). In line with our findings in *C. elegans*, DAVID enrichment analyses showed cytoprotective processes to have high TEs, developmental processes to have low TEs, and visual inspection confirmed the near total suppression of RP genes' TEs (Figure S3C, Table S6). Taken together, these findings indicate that *in vivo* pharmacological inhibition of mitochondrial translation co-suppresses cytoplasmic translation, directly reducing cytoplasmic RP transcript TE. This confirms that the mechanism for balancing mitochondrial and cytoplasmic translation is conserved from nematodes to mammals.

Having observed a strong conservation of the molecular phenotypes in *mrps-5* RNAi treated worms and doxycycline-treated mouse livers, we next asked what molecular signatures were specifically conserved between the two models. To do so, we performed a mouse-worm cross-species comparison of both total and polysomal RNA-seq libraries for orthologous genes (Figure 5G). Total and polysomal RNA abundances showed interspecies correlations of 0.42 and 0.39, respectively. Assessing the overlap of differentially expressed murine and *C. elegans* genes (Figure 5H) showed a conserved upregulation of genes coding for mitochondrial transit peptides and oxidation reduction in the total RNA and a downregulation of genes involved in mRNA translation in the polysomal RNA (Table S7).

Taken all together, our findings suggest that a conserved program for mito-cytoplasmic translational balance is activated across species when mitochondrial translation is inhibited by distinct and diverse methods. Our findings demonstrate that this leads to ATF4/*atf-5* mediated signaling to slow down cytoplasmic translation while upregulating cyto-protective genes. Considering the remarkable longevity induced by *mrps-5* and doxycycline treatments (Houtkooper et al., 2013), we propose that mito-cytoplasmic translational balance can ultimately be used to assure longevity for the organism (Figure 5I).

Discussion

In this study we used a systems biology approach operating on multiple levels of biology to elucidate the relationship between mitochondrial and cytoplasmic translation. This included analyzing mouse population transcriptomics, worm proteome-transcriptome regulation, and polysome fractionated transcriptomics from both worms and mice with impaired mitochondrial ribosomes. Through this approach, we identified a mito-cytoplasmic translational balance whereby the functional ability and abundance levels of mitochondrial ribosomes are communicated to the cytoplasmic ribosomes to suppress cytoplasmic translation. This was found conserved across species and in different genetic backgrounds. Furthermore, we have shown evidence that this communication is dependent on the transcription factor ATF4. Taken together, our work establishes the presence of a retrograde communication process between mitochondrial and cytoplasmic ribosomes.

Communication occurring from the cytoplasmic ribosomes regulates mitochondrial protein abundance (Couvillion et al., 2016; Fujiki and Verner, 1993; Surguchov et al., 1983). Indeed, mitochondria are dependent on cytoplasmic translation, as the vast majority of the ~1200 mitochondrial proteins, including mitochondrial RPs, are synthesized by cytoplasmic ribosomes (Attimonelli et al., 2002). However, given the energy requirement for cytoplasmic ribosome

biogenesis and function coupled to the mitochondrial function as the main source of cellular energy, a clear need exists for the cytoplasmic and mitochondrial ribosomes to communicate their operational state to each other. Indeed, evidence for other mechanisms of communication from the mitochondria to the nucleus has been well documented. When a mitonuclear protein imbalance occurs due to inhibition of mitochondrial translation, the UPR^{mt} is activated which triggers a nuclear transcriptional response to ultimately restore mitochondrial proteostasis (Haynes and Ron, 2010; Houtkooper et al., 2013). However, the effect on cytoplasmic proteostasis in a situation where mitochondrial translation was inhibited was still unclear. Also, a cytoplasmic proteostatic response occurs when mitochondrial proteins are not properly targeted to mitochondria and erroneously accumulate in the cytoplasm (Wrobel et al., 2015). Similarly, it has been shown that defective mitochondrial tRNA taurine modifications can also result in global cellular proteostasis activation mechanisms (Fakruddin et al., 2018), which again points to an intrinsic protein homeostasis network between the mitochondria and cytosol. Indeed, our work builds upon these prior observations of inter-organelle communication and establishes the ribosomes as cross-communicating complexes between subcellular organelles.

Our findings provide a framework to better understand prior observations in mitochondrial biology. For example, dysfunction in mitochondrial ribosomes was shown to block cell proliferation prior to any loss of mitochondrial respiration (Richter et al., 2013). Our findings suggest that the mito-to-cytoplasmic translation balance could play a role in this anti-proliferation signal from the mitochondrial ribosomes by slowing down cytoplasmic translation. Similarly, our findings can help explain the anti-carcinogenic activity of antibiotics such as doxycycline and tigecycline (Kuntz et al., 2017; Skrtic et al., 2011). With cytoplasmic translation already established as a target for cancer therapy (Faller et al., 2015), our work points to the possibility that this could be achieved through the cellular mechanisms in place to achieve mito-to-cytoplasmic translation balance.

The loss of respiration is one of the downstream effects of impaired mitochondrial translation in the *mrps-5* worms (Houtkooper et al., 2013). Though we observed a strong upregulation of mitochondrial OXPHOS on the transcript level, we observed at the protein level that OXPHOS components were downregulated, explaining the loss of respiration observed in the worms. OXPHOS in the mitochondria is carried out by five different protein complexes, of which four are dependent on mtDNA-encoded subunits. Interestingly, the proteins that were up on the transcript level and down on protein level (such as *nuo-6*, *nuo-3*, *nuo-2*, *nduf-7* and *nduf-6*) were mainly nuclear-encoded OXPHOS complex I proteins, which is the complex dependent on the most (seven) mtDNA-encoded proteins. This suggests that the *mrps-5* worms may be trying to redress their loss of respiration by upregulating translation of mitochondrial proteins, however, due to the lack of translation of their mtDNA-encoded partners those OXPHOS complexes cannot assemble and proteins are degraded. This, in turn, may aggravate mitochondrial proteotoxic stress.

We found that *Atf4* plays a role in orchestrating the communication from the mitoribosome to the cytoribosome. Interestingly, upregulation of this transcription factor has been linked to longevity in mice (Li et al., 2014) and overexpression of the orthologous transcription factor in yeast (*GCN4*) extended lifespan (Mittal et al., 2017), both in line with observations that *mrps-5* RNAi-treated worms are longer lived (Houtkooper et al., 2013). In the yeast overexpression study, it was observed that *Gcn4* acts as a repressor of protein synthesis (Mittal et al., 2017), in line with our observations in nematode and mammalian models. While the regulation of *Atf4* and its orthologues *Gcn4* and *atf-5* is not fully understood, it is known that differential contribution of two upstream ORFs (uORFs) in the 5' leader of the mouse *Atf4* mRNA regulates *Atf4* expression (Vattem and Wek, 2004), and understanding more on how *Atf4* activation is regulated may be valuable to target the aging process.

Our cross-species analyses resulted in a transcriptional signature that was changing similarly in both worms and mice upon inhibition of mitochondrial translation. Most of the upregulated hits in our signature were mitochondrial proteins suggesting a mitochondrial quality control system. This signature involved cytoprotective transcriptional changes, including an upregulation of oxidation-reduction processes, and was characterized by a reduction of translation EFs. These findings are in line with the observation that inhibiting mitochondrial translation is a conserved longevity mechanism (Houtkooper et al., 2013). Our work here shows that this inhibition can also induce a previously unknown mito-cytoplasmic translational balance whereby cytoplasmic translation is also lowered, linking to another longevity mechanism (MacInnes, 2016). Finally, we identified a cyto-protective transcriptional signature characteristic of this response, and together these changes have the potential to drive healthy aging (Figure 5I).

Acknowledgements

Work in the Houtkooper group is financially supported by an ERC Starting grant (no. 638290), a VIDI grant from ZonMw (no. 91715305), and a grant from the Velux Stiftung (no. 1063). AWM is supported by E-Rare-2, the ERA-Net for Research on Rare Diseases (ZonMW #40-44000-98-1008). GEJ is supported by a 2018 Federation of European Biochemical Society (FEBS) long-term fellowship. EGW was supported by an NIH F32 Ruth Kirchstein Fellowship (F32GM119190). RA was supported by the European Research Council advanced grant ERC-20140AdG 670821.

Author contributions

MM, GEJ, AWM, and RHH conceived and designed the project. MM, SR, FJ, and JL performed experiments and GEJ, EGW, AJ, PM, and AK performed bioinformatics. MM, GEJ, EGW, AWM, and RHH interpreted data. MM, GEJ, AWM and RHH wrote the manuscript, with contributions from all other authors.

Conflict of interest

RHH is an inventor on a patent related to mitochondrial ribosomal proteins as aging regulators.

The other authors declare that they have no conflict of interest.

References

- Anders, S., Pyl, P.T., and Huber, W. (2015). HTSeq--a Python framework to work with high-throughput sequencing data. *Bioinformatics (Oxford, England)* 31, 166-169.
- Andrews, S. (2010). FastQC: a quality control tool for high throughput sequence data. Available online at: <http://www.bioinformatics.babraham.ac.uk/projects/fastqc>.
- Attimonelli, M., Catalano, D., Gissi, C., Grillo, G., Licciulli, F., Liuni, S., Santamaria, M., Pesole, G., and Saccone, C. (2002). MitoNuc: a database of nuclear genes coding for mitochondrial proteins. Update 2002. *Nucleic acids research* 30, 172-173.
- Bolger, A.M., Lohse, M., and Usadel, B. (2014). Trimmomatic: a flexible trimmer for Illumina sequence data. *Bioinformatics (Oxford, England)* 30, 2114-2120.
- Boulesteix, A.L., and Strimmer, K. (2007). Partial least squares: a versatile tool for the analysis of high-dimensional genomic data. *Briefings in bioinformatics* 8, 32-44.
- Buttgereit, F., and Brand, M.D. (1995). A hierarchy of ATP-consuming processes in mammalian cells. *The Biochemical journal* 312 (Pt 1), 163-167.
- Chiocchetti, A., Zhou, J., Zhu, H., Karl, T., Haubenreisser, O., Rinnerthaler, M., Heeren, G., Oender, K., Bauer, J., Hintner, H., *et al.* (2007). Ribosomal proteins Rpl10 and Rps6 are potent regulators of yeast replicative life span. *Experimental gerontology* 42, 275-286.
- Couvillion, M.T., Soto, I.C., Shipkovenska, G., and Churchman, L.S. (2016). Synchronized mitochondrial and cytosolic translation programs. *Nature* 533, 499-503.
- Fakruddin, M., Wei, F.Y., Suzuki, T., Asano, K., Kaieda, T., Omori, A., Izumi, R., Fujimura, A., Kaitsuka, T., Miyata, K., *et al.* (2018). Defective Mitochondrial tRNA Taurine Modification Activates Global Proteostress and Leads to Mitochondrial Disease. *Cell reports* 22, 482-496.
- Faller, W.J., Jackson, T.J., Knight, J.R., Ridgway, R.A., Jamieson, T., Karim, S.A., Jones, C., Radulescu, S., Huels, D.J., Myant, K.B., *et al.* (2015). mTORC1-mediated translational elongation limits intestinal tumour initiation and growth. *Nature* 517, 497-500.
- Fujiki, M., and Verner, K. (1993). Coupling of cytosolic protein synthesis and mitochondrial protein import in yeast. Evidence for cotranslational import in vivo. *The Journal of biological chemistry* 268, 1914-1920.
- Greber, B.J., Bieri, P., Leibundgut, M., Leitner, A., Aebersold, R., Boehringer, D., and Ban, N. (2015). Ribosome. The complete structure of the 55S mammalian mitochondrial ribosome. *Science (New York, NY)* 348, 303-308.
- Greber, B.J., Boehringer, D., Leibundgut, M., Bieri, P., Leitner, A., Schmitz, N., Aebersold, R., and Ban, N. (2014). The complete structure of the large subunit of the mammalian mitochondrial ribosome. *Nature* 515, 283-286.
- Hansen, M., Taubert, S., Crawford, D., Libina, N., Lee, S.J., and Kenyon, C. (2007). Lifespan extension by conditions that inhibit translation in *Caenorhabditis elegans*. *Aging cell* 6, 95-110.

- Haynes, C.M., and Ron, D. (2010). The mitochondrial UPR - protecting organelle protein homeostasis. *Journal of cell science* 123, 3849-3855.
- Houtkooper, R.H., Mouchiroud, L., Ryu, D., Moullan, N., Katsyuba, E., Knott, G., Williams, R.W., and Auwerx, J. (2013). Mitonuclear protein imbalance as a conserved longevity mechanism. *Nature* 497, 451-457.
- Huang da, W., Sherman, B.T., and Lempicki, R.A. (2009). Systematic and integrative analysis of large gene lists using DAVID bioinformatics resources. *Nature protocols* 4, 44-57.
- Jovaisaite, V., and Auwerx, J. (2015). The mitochondrial unfolded protein response-synchronizing genomes. *Current opinion in cell biology* 33, 74-81.
- Kim, D., Langmead, B., and Salzberg, S.L. (2015). HISAT: a fast spliced aligner with low memory requirements. *Nature methods* 12, 357-360.
- Kuhn, A., Luthi-Carter, R., and Delorenzi, M. (2008). Cross-species and cross-platform gene expression studies with the Bioconductor-compliant R package 'annotationTools'. *BMC bioinformatics* 9, 26.
- Kuntz, E.M., Baquero, P., Michie, A.M., Dunn, K., Tardito, S., Holyoake, T.L., Helgason, G.V., and Gottlieb, E. (2017). Targeting mitochondrial oxidative phosphorylation eradicates therapy-resistant chronic myeloid leukemia stem cells. *Nature medicine* 23, 1234-1240.
- Lane, N., and Martin, W. (2010). The energetics of genome complexity. *Nature* 467, 929-934.
- Law, C.W., Chen, Y., Shi, W., and Smyth, G.K. (2014). voom: Precision weights unlock linear model analysis tools for RNA-seq read counts. *Genome biology* 15, R29.
- Li, W., Li, X., and Miller, R.A. (2014). ATF4 activity: a common feature shared by many kinds of slow-aging mice. *Aging cell* 13, 1012-1018.
- MacInnes, A.W. (2016). The role of the ribosome in the regulation of longevity and lifespan extension. *Wiley interdisciplinary reviews RNA* 7, 198-212.
- Mittal, N., Guimaraes, J.C., Gross, T., Schmidt, A., Vina-Vilaseca, A., Nedialkova, D.D., Aeschmann, F., Leidel, S.A., Spang, A., and Zavolan, M. (2017). The Gcn4 transcription factor reduces protein synthesis capacity and extends yeast lifespan. *Nature communications* 8, 457.
- Molenaars, M., Janssens, G.E., Santermans, T., Lezzerini, M., Jelier, R., MacInnes, A.W., and Houtkooper, R.H. (2018). Mitochondrial ubiquinone-mediated longevity is marked by reduced cytoplasmic mRNA translation. *Life science alliance* 1.
- Moullan, N., Mouchiroud, L., Wang, X., Ryu, D., Williams, E.G., Mottis, A., Jovaisaite, V., Frochaux, M.V., Quiros, P.M., Deplancke, B., *et al.* (2015). Tetracyclines Disturb Mitochondrial Function across Eukaryotic Models: A Call for Caution in Biomedical Research. *Cell reports*.
- Narayan, V., Ly, T., Pourkarimi, E., Murillo, A.B., Gartner, A., Lamond, A.I., and Kenyon, C. (2016). Deep Proteome Analysis Identifies Age-Related Processes in *C. elegans*. *Cell systems* 3, 144-159.

- Neuwirth, E. (2014). RColorBrewer: ColorBrewer Palettes. R package version 1.1-2. <https://CRAN.R-project.org/package=RColorBrewer>.
- Pan, K.Z., Palter, J.E., Rogers, A.N., Olsen, A., Chen, D., Lithgow, G.J., and Kapahi, P. (2007). Inhibition of mRNA translation extends lifespan in *Caenorhabditis elegans*. *Aging cell* 6, 111-119.
- Parker, S.J., Rost, H., Rosenberger, G., Collins, B.C., Malmstrom, L., Amodei, D., Venkatraman, V., Raedschelders, K., Van Eyk, J.E., and Aebersold, R. (2015). Identification of a Set of Conserved Eukaryotic Internal Retention Time Standards for Data-independent Acquisition Mass Spectrometry. *Molecular & cellular proteomics : MCP* 14, 2800-2813.
- Quiros, P.M., Prado, M.A., Zamboni, N., D'Amico, D., Williams, R.W., Finley, D., Gygi, S.P., and Auwerx, J. (2017). Multi-omics analysis identifies ATF4 as a key regulator of the mitochondrial stress response in mammals. *The Journal of cell biology* 216, 2027-2045.
- Richter, U., Lahtinen, T., Marttinen, P., Myohanen, M., Greco, D., Cannino, G., Jacobs, H.T., Lietzen, N., Nyman, T.A., and Battersby, B.J. (2013). A mitochondrial ribosomal and RNA decay pathway blocks cell proliferation. *Current biology : CB* 23, 535-541.
- Ritchie, M.E., Phipson, B., Wu, D., Hu, Y., Law, C.W., Shi, W., and Smyth, G.K. (2015). limma powers differential expression analyses for RNA-sequencing and microarray studies. *Nucleic acids research* 43, e47.
- Robinson, M.D., McCarthy, D.J., and Smyth, G.K. (2010). edgeR: a Bioconductor package for differential expression analysis of digital gene expression data. *Bioinformatics (Oxford, England)* 26, 139-140.
- Rohart, F., Gautier, B., Singh, A., and Le Cao, K.A. (2017). mixOmics: An R package for 'omics feature selection and multiple data integration. *PLoS computational biology* 13, e1005752.
- Rost, H.L., Rosenberger, G., Navarro, P., Gillet, L., Miladinovic, S.M., Schubert, O.T., Wolski, W., Collins, B.C., Malmstrom, J., Malmstrom, L., *et al.* (2014). OpenSWATH enables automated, targeted analysis of data-independent acquisition MS data. *Nature biotechnology* 32, 219-223.
- Skrtic, M., Sriskanthadevan, S., Jhas, B., Gebbia, M., Wang, X., Wang, Z., Hurren, R., Jitkova, Y., Gronda, M., Maclean, N., *et al.* (2011). Inhibition of mitochondrial translation as a therapeutic strategy for human acute myeloid leukemia. *Cancer cell* 20, 674-688.
- Smits, P., Smeitink, J.A., van den Heuvel, L.P., Huynen, M.A., and Ettema, T.J. (2007). Reconstructing the evolution of the mitochondrial ribosomal proteome. *Nucleic acids research* 35, 4686-4703.
- Surguchov, A.P., Sudarickov, A.B., Telckov, M.V., Smirnov, V.N., Ter-Avanesyan, M.D., and Inge-Vechtomov, S.G. (1983). Relationship between cytoplasmic and mitochondrial apparatus of protein synthesis in yeast *Saccharomyces cerevisiae*. *Molecular & general genetics : MGG* 189, 172-174.
- Vattem, K.M., and Wek, R.C. (2004). Reinitiation involving upstream ORFs regulates ATF4 mRNA translation in mammalian cells. *Proceedings of the National Academy of Sciences of the United States of America* 101, 11269-11274.

Wang, X., Pandey, A.K., Mulligan, M.K., Williams, E.G., Mozhui, K., Li, Z., Jovaisaite, V., Quarles, L.D., Xiao, Z., Huang, J., *et al.* (2016). Joint mouse-human phenome-wide association to test gene function and disease risk. *Nature communications* 7, 10464.

Warnes, G.R., Bolker, B., Bonebakker, L., Gentleman, R., Huber, W., Liaw, A., Lumley, T., Maechler, M., Magnusson, A., Moeller, S., *et al.* (2016). *gplots: Various R Programming Tools for Plotting Data*. R package version 3.0.1. <https://CRAN.R-project.org/package=gplots>.

Wickham, H. (2009). *ggplot2: Elegant Graphics for Data Analysis* Springer-Verlag New York.

Wieser, W., and Krumschnabel, G. (2001). Hierarchies of ATP-consuming processes: direct compared with indirect measurements, and comparative aspects. *The Biochemical journal* 355, 389-395.

Williams, E.G., Wu, Y., Jha, P., Dubuis, S., Blattmann, P., Argmann, C.A., Houten, S.M., Amariuta, T., Wolski, W., Zamboni, N., *et al.* (2016). Systems proteomics of liver mitochondria function. *Science (New York, NY)* 352, aad0189.

Williams, E.G., Wu, Y., Wolski, W., Kim, J.Y., Lan, J., Hasan, M., Halter, C., Jha, P., Ryu, D., Auwerx, J., *et al.* (2018). Quantifying and Localizing the Mitochondrial Proteome Across Five Tissues in A Mouse Population. *Molecular & cellular proteomics : MCP* 17, 1766-1777.

Wrobel, L., Topf, U., Bragoszewski, P., Wiese, S., Sztolsztener, M.E., Oeljeklaus, S., Varabyova, A., Lirski, M., Chroscicki, P., Mroczek, S., *et al.* (2015). Mistargeted mitochondrial proteins activate a proteostatic response in the cytosol. *Nature* 524, 485-488.

Wu, Y., Williams, E.G., and Aebersold, R. (2017). Application of SWATH Proteomics to Mouse Biology. *Current protocols in mouse biology* 7, 130-143.

Figure legends

Figure 1. A conserved mito-cyto translational balance in mice and worms.

(A) Model showing possible links between two branches of translation regulation in lifespan control; cytoplasmic (yellow) and mitochondrial (blue).

(B) Correlation networks in BXD mice show strong relationships between mitochondrial and cytoplasmic ribosomal protein levels both in liver (left) and across multiple tissues (right), suggesting that the subunits within ribosomes and across ribosomes are coregulated. Both networks show enriched connectivity. Liver: 73 nodes for the cytoribosome subnetwork have 610 edges ($p < 1e-4$, 512 are positively correlated), 38 nodes for the mitoribosome subnetwork have 88 edges ($p = 0.014$, 57 are positively correlated), 374 nodes are involved in the interaction between mitoribosome and cytoribosome subnetworks ($p < 1e-4$, 211 are positively correlated). Multitissue: 68 nodes for the cytoribosome subnetwork have 1441 edges ($p < 1e-4$, 1441 are positively correlated), 55 nodes for the mitoribosome subnetwork have 491 edges ($p < 1e-4$, 491 are positively correlated), 703 nodes are involved in the interaction between mitoribosome and cytoribosome subnetworks ($p < 1e-4$, 680 are positively correlated). For significance testing, 10,000 random networks were permuted using the same input data and gene set size for each data set and subset with gene sets of the same size selected at random out of the full proteomic datasets. A reported $p < 1e-4$ means that none of the 10,000 random networks were as significant as the selected ribosome gene sets taken from literature.

(C) BXD mouse strains showing natural variation in cytoplasmic (yellow) or mitochondrial (blue) ribosome abundances in liver proteome. Each dot represents one BXD strain's average abundance of either the cytoplasmic or mitochondrial ribosomes.

(D) Averaged abundances from mitochondrial and cytoplasmic ribosomes in the BXD liver proteome (from (C)) show correlation between mitochondrial and cytoplasmic abundances (Pearson 0.60, $p < 7e-5$).

(E) Representative polysome profiles showing decreased cytoplasmic polysome abundances in worms with impaired mitochondrial ribosomal biogenesis (*mrps-5* RNAi). Lysate is normalized to protein levels. The subunits (40S and 60S), monosomal peak (80S), and polysomal peak numbers are indicated (P1–P6).

(F) Quantification of polysome peak sizes of representative experiment with N=4 per condition normalized to P1 peak of empty vector control worms. Error bars represent mean \pm SD and significance was tested with Student's t-test, and *p*-values were adjusted to correct for multiple testing using the Holm-Šidák method, with $\alpha = 0.05$.

See also Table S1.

Figure 2. *mrps-5* RNAi-treated worms show reduced translational efficiencies for cytoplasmic ribosomal genes.

(A) Schematic showing RNA isolated from polysome profiles, from highly translated fractions (yellow, polysome), and lesser translated fractions (blue, monosome). RNA-seq transcriptomics was performed on polysomal and monosomal fractions for *mrps-5* RNAi and control worms. Transcripts (log₂ transformed normalized counts) are depicted (scatterplots). Biological triplicates were used for each condition.

(B-C) Partial least squares discriminant analysis (PLS-DA) for monosomal (B) and polysomal (C) RNA libraries showing clear distinction between *mrps-5* RNAi and control samples. Analysis was used to derive VIP scores, for genes contributing most to the group separation.

(D) Translational efficiencies (TE) of transcripts, defined as the log₂ ratio of polysomal vs monosomal differences between *mrps-5* RNAi and control gene expression, shows shifts in transcripts from either the monosome to the polysome (high TE, yellow) or the polysome to the monosome (low TE, blue). Insets schematically depict the shifts observed in the histogram. Cutoff lines and VIP scores were used to remove noise for calculating enrichment of biological processes in low or high TE mRNAs.

(E) Top 10 biological processes with highest enrichments scores in low TE (blue) or high TE (yellow) transcripts using DAVID analysis clusters enrichments in Gene Ontologies (GO). Decreased TE was observed in pathways such as ribosome biogenesis and translation. Clusters with an 'Enrichment Score' above 1.3 ($p < 0.05$, indicated with dotted line) were considered significantly enriched.

(F) Selection of mRNAs with either low TE (blue) or high TE (yellow), which contributed to the biological enrichments ('translation' or 'integral component of membrane,' respectively). Boxplots depict abundances (counts per million) of mRNA in the monosome and polysome for control and *mrps-5* RNAi treated worms, used to calculate TEs.

(G) Individual cytoplasmic ribosomal proteins have a low TE in *mrps-5* RNAi compared to control worms.

See also Figure S1 and Table S2.

Figure 3. Proteome-transcriptome cross-comparison of *mrps-5* RNAi worms reveals transcriptional suppression of growth pathways and upregulation of stress responses.

(A) Schematic showing RNA (light blue) and proteins (light green) isolated from whole worms for RNA-seq or SWATH proteomics. Transcripts or proteins (Log₂-transformed normalized counts) are depicted (scatterplots). RNA-seq was performed in biological triplicates and proteomics performed in biological quintuple per condition.

(B-C) Partial least squares discriminant analysis (PLS-DA) for transcriptome (B) and proteome (C) shows clear distinction between *mrps-5* RNAi and control samples. PLS-DA was used to derive VIP scores, for genes contributing most to the group separation.

(D-E) Significant correlations of 0.44 and 0.43 were observed in the fold changes between the 1407 transcript-protein pairs overlapping the mRNA-protein datasets for control (D) and *mrps-5* RNAi (E) samples respectively.

(F) Co-regulation plot of transcript and protein fold changes of *mrps-5* RNAi vs control samples. Quadrants are defined as Q1 co-upregulated, Q2, post-transcriptionally increased, Q3 co-downregulated, and Q4, post-transcriptionally suppressed. Dashed lines indicate cutoff used to eliminate noise of near zero fold change (mRNA and protein cutoffs each relative to the standard deviation of their distributions), and a VIP score > 1 for both mRNA and protein levels were considered as significant hits. Pie chart inset shows percentage regulated, revealing a majority of changes being co-regulated.

(G) Examples of co-upregulated, co-downregulated, or post-transcriptionally suppressed genes, derived from the significant hits of panel (F).

(H-K) Top 5 biological processes enriched in each quadrant of the co-regulation plot, derived from the significant hits of panel (F).

See also Tables S3-5.

Figure 4. *Atf4/atf-5* mediates the balance between mitochondrial and ribosomal protein translation.

(A) Representative polysome profiles of control (black), *mrps-5* RNAi (red), and *mrps-5* RNAi + *atf-5* RNAi (yellow) worms shows *mrps-5* mediated cytoplasmic translational suppression is dependent on the *atf-5* transcription factor. Lysate is normalized to protein levels. The subunits (40S and 60S), monosomal peak (80S), and polysomal peak numbers are indicated (P1–P6).

(B) Quantification of polysome peak sizes of representative experiment with N=4 per condition normalized to P1 peak of empty vector control worms. Bars represent mean \pm SD and significance was tested with Student's t-test, and p-values were adjusted to correct for multiple testing using the Holm-Šídák method, with $\alpha = 0.05$.

(C) Schematic of doxycycline (DOX) mediated inhibition of mitochondrial ribosomes with amoxicillin not interfering with mitochondria as control antibiotic.

(D) Polysome profiles of DMSO and amoxicillin (AMOX) controls and doxycycline (DOX)-treated K562 cells shows doxycycline-induced suppression of cytoplasmic translation.

(E) Western blot analyses of amoxicillin control and doxycycline-treated K562 cells shows doxycycline-induced expression of ATF4. Bars represent mean \pm SD and significance was tested with 1way ANOVA with multiple comparisons, with $\alpha = 0.05$

Figure 5. Suppressing mitochondrial ribosomes by doxycycline treatment suppresses cytoplasmic ribosome abundance *in vivo* in mice liver, resulting in a conserved transcriptional signature for longevity assurance.

(A) Schematic showing RNA isolated from either the polysomal fraction or total RNA, from livers of germ-free mice treated with either doxycycline (DOX, red) or amoxicillin control (AMOX, black). Transcripts (Log2 transformed normalized counts) are depicted (scatterplots). For RNA-seq, biological triplicates were used for each condition.

(B-C) Partial least squares discriminant analysis (PLS-DA) for total (B) and polysomal (C) RNA libraries showing clear distinction between amoxicillin- and doxycycline-treated samples. Analysis was used to derive VIP scores, for genes contributing most to the group separation.

(D-E) Downregulated (D) or upregulated (E) top 10 biological processes enriched in the polysomal RNA of doxycycline-treated mice compared to amoxicillin, shows a suppression of translation-related transcripts after doxycycline treatment. A VIP score > 1 was used to identify differentially expressed genes.

(F) Individual cytoplasmic ribosomal proteins are downregulated in the polysomal RNA in doxycycline-treated mouse livers.

(G-H) Mouse-worm cross species comparison of total and polysomal RNA-seq libraries reveals a conserved transcriptional response for a polysomal downregulation of 'mRNA translation'-related proteins and total RNA upregulation of 'mito transit peptides' and 'oxidation reduction' related genes.

(I) Model depicting how downregulating mitochondrial translation results in a coordinated downregulation of cytoplasmic translation via *Atf4/atf-5*, along with an upregulation of oxidation-reduction genes pathways ultimately leading towards longevity for the organism.

See also Figure S2-3 and Tables S6-7.

Supplemental figure legends

Figure S1. VIP score correlates highly to traditional *p*-value ranking, related to Figure 2;

Table S2

(A-B) Partial least squares discriminant analysis (PLS-DA) derived a variable of importance (VIP) score for each gene. Bayes moderated *t*-test used to derive *p* values. Performed for both (A) monosomal and (B) polysomal RNAseq results.

Figure S2. Doxycycline treatment resulted in suppression of global translation in liver in a dose-dependent manner, related to figure 5.

(A) Representative polysome profiles showing decreased cytoplasmic polysome abundances in the liver of mice treated with either a low dose of doxycycline (50 mg/kg/d) or a high dose of doxycycline (500 mg/kg/d) compared to control amoxicillin-treated mice (50 mg/kg/d). Lysate is normalized to protein levels.

(B) Quantification of polysome peak sizes with N=3 mice per condition normalized to P1 peak of amoxicillin-treated mice. Bars represent mean \pm SD and significance was tested with Student's *t*-test, and *p*-values were adjusted to correct for multiple testing using the Holm-Šídák method, with $\alpha = 0.05$.

Figure S3. Translational efficiency (TE) plot Dox mice and individual cytoplasmic and mitochondrial ribosomal proteins, Related to figure 5; Table S6

(A) Translational efficiencies (TE) of transcripts, defined as the log₂ ratio of polysomal vs total differences between doxycycline-treated mice (50 mg/kg/d) and control amoxicillin-treated mice (50 mg/kg/d) gene expression, shows shifts in transcripts from either the monosome to the polysome (high TE, yellow) or the polysome to the monosome (low TE, blue).

(B) Fold changes of individual cytoplasmic ribosomal proteins in the total RNA in doxycycline-treated mouse livers.

(C) Individual cytoplasmic ribosomal proteins have a low TE in doxycycline-treated mice (50 mg/kg/d) compared to control amoxicillin-treated mice. TE of transcripts defined as the log₂ ratio of polysomal vs monosomal differences between doxycycline-treated (50 mg/kg/d) and amoxicillin-treated mice gene expression.

(D) Fold changes of individual mitochondrial ribosomal proteins in the total RNA in doxycycline-treated mouse livers.

(E) Fold changes of individual mitochondrial ribosomal proteins in the polysomal RNA in doxycycline-treated mouse livers.

STAR methods

CONTACT FOR REAGENT AND RESOURCE SHARING

Further information and requests for resources and reagents should be directed to and will be fulfilled by the Lead Contact, Riekelt H. Houtkooper (r.h.houtkooper@amc.nl).

EXPERIMENTAL MODEL AND SUBJECT DETAILS

Nematode growing conditions and RNAi experiments

Worms were cultured at 20°C on nematode growth medium (NGM) agar plates seeded with OP50 strain *Escherichia coli* as described before (Molenaars et al., 2018). Synchronized N2 worms were harvested and snap frozen at L4 larval stage for either total mRNA isolation, polysome profiling, or proteomics. For RNAi knock down experiments, 5000 synchronized eggs were plated on NGMi (containing 2 mM IPTG) with a bacterial lawn of either *E. coli* HT115 (RNAi control strain, containing an empty vector) or *mrps-5*, *atf-5* RNAi bacteria from the Ahringer *C. elegans* RNAi library.

K562 cell culture

K562 cells were cultured on 37°C in antibiotic-free RPMI 1640 medium (Thermo Fischer Scientific) supplemented with 10% FBS (Bodinco) and 25 mM HEPES (VWR Life Science) . After 48 treatment with either 20 µM amoxicillin (Sigma), 20 µM doxycycline (Sigma), or DMSO (Sigma) as a vehicle control (0.05% in media), cells were harvested for western blotting or polysome profiling.

C57BL/6J germ-free mice

C57BL/6J germ-free male mice were housed 4 animals per cage and randomly assigned to the 3 experimental groups with N=8 mice per treatment. At the age of 9 weeks mice were treated for two weeks with either amoxicillin (50 mg/kg/d), or one of two doses of doxycycline (50 mg/kg/d or 500 mg/kg/d) in the drinking water supplemented with 5% sucrose. Mice were sacrificed after 12

hours of fasting, and the livers were harvested and snap frozen in liquid N₂. Liver tissue (~20 mg) was ground in liquid N₂ in a mortar and pestle and used for either mRNA isolation or polysome profiling. Procedures were carried out in accordance with the European guidelines for the care and use of laboratory animals; they were approved by the Ethics Committee of AgroParisTech and the INRA Research Center of Jouy-en-Josas (approval reference: 14–40).

METHOD DETAILS

BXD strains

The BXD mouse liver proteome data used for network analyses were used from a prior publication (Williams et al., 2016) that consists of 73 cohorts of BXD mice—38 strains on chow diet and 35 strains on high fat diet for proteomics, and were combined. Note that the raw liver proteomics data from PXD003266 from 2016 were re-analyzed using the newer SWATH search library from PXD005044 from 2018, which was designed to improve coverage for mitochondrial proteins. These re-processed and normalized and processed mouse data are also available as Supplemental table 1. BXD mouse multi-tissue data were used from a prior publication (Williams et al., 2018) using datasets available in the Gene Expression Omnibus (GEO; GSE60149, GSE60150, GSE60151, and GSE60489). BXD mouse liver proteome data for average abundance quantification (Fig 1C-D) were downloaded from www.genenetwork.org (GN540).

Network analysis

Correlation network graphs were calculated using the above-referenced BXD proteome data using the iGraph v1.2.1 package in R. In the liver proteomics data, 77 cohorts were measured. 73 distinct cytoplasmic ribosome genes were quantified while 38 distinct mitochondrial ribosome genes were quantified. In the cross-tissue data, 40 samples from 5 tissues were measured. The cytoplasmic ribosome had 68 proteins quantified, while the mitochondrial ribosome had 55 proteins quantified. A fixed p-value cutoff for both networks was used ($p < 5e-4$), with varying corresponding *rho* due

to varying n . Note that protein expression is generally more highly variable across 40 samples from 5 tissues than it is across 77 samples just from liver. Nodes that have 0 or 1 edge connection to the rest of the network were visually suppressed, but are still counted in the edge and node counts reported. For significance testing, 10,000 random networks were permuted using the same input data and gene set size for each data set and subset with gene sets of the same size selected at random out of the full proteomic datasets. A reported $p < 1e-4$ means that none of the 10,000 random networks were as significant as the selected ribosome gene sets taken from literature. Testing was only performed for overall edge counts.

Polysome profiling

Gradients of 17–50% sucrose (11 ml) in gradient buffer (110 mM KAc, 20 mM MgAc₂ and 10 mM HEPES pH 7.6) were prepared on the day before use in thin-walled, 13.2 ml polypropylene (14 x 89 mm) centrifuge tubes (Beckman-Coulter, USA). Nematodes were lysed in 500 ml polysome lysis buffer (gradient buffer containing 100 mM KCl, 10 mM MgCl₂, 0.1% NP-40, 2 mM DTT, 0.5 mM cycloheximide and RNaseOUT™ (Thermo Fischer Scientific) using a Dounce homogenizer (Wheaton, USA) as described before (Molenaars et al., 2018). Mouse livers and K562 cells were lysed similarly with polysome lysis buffer but containing 5 mM cycloheximide. The samples were centrifuged at 1200 g for 10 min to remove debris and the supernatant was subjected to BCA protein assay (company). In all, 500 µg of total protein for each sample was loaded on top of the sucrose gradients. The gradients were ultra-centrifuged for 2 h at 40,000 g in a SW41Ti rotor (Beckman-Coulter, USA). The gradients were displaced into a UA6 absorbance reader (Teledyne ISCO, USA) using a syringe pump (Brandel, MD, USA) containing 60% sucrose. Absorbance was recorded at an OD of 254 nm. All steps of this assay were performed at 4°C or on ice and all chemicals came from Sigma-Aldrich (St. Louis, MO, USA) unless stated otherwise. Polysome peaks were quantified by measuring area under the curve (AUC) in ImageJ. Significance was

tested with Student's t-test, and p-values were adjusted to correct for multiple testing using the Holm-Šídák method, with alpha = 0.05.

Western blotting

For extraction of protein, K562 pellets were resuspended in RIPA buffer with cOmplete Mini Protease Inhibitor Cocktail (Sigma-Aldrich). Lysates were incubated on ice for 10 minutes and then centrifuged at 16,000 x g for 10 minutes in a pre-chilled centrifuge to remove debris and quantification was carried out with BCA protein assay. Equal amounts of protein (25-50 µg) were loaded onto NuPAGE® Novex 4-12% Bis-Tris Gel 1.5 mm, 10 Well (Invitrogen) and subsequently transferred to nitrocellulose membranes using iBlot™ 2 Transfer Stacks (Invitrogen) for 7 minutes at 14 V in iBlot™ 2 Dry Blotting System (Invitrogen). Western blotting was performed with antibodies against ATF4 (Cell Signaling Technology, #11815), β-actin (Sigma-Aldrich, #A5441), IRDye® 680RD Donkey anti-Rabbit secondary antibody (Li-Cor, #925-68073), and IRDye® 800CW Goat anti-Mouse secondary antibody (Li-Cor, #925-32210) and visualized using the Odyssey® Imaging System.

Isolation of mRNA (Total, Monosomal, and Polysomal)

For isolation of total mRNA, whole worms or liver tissue were homogenized with a 5 mm steel bead using a TissueLyser II (Qiagen) for 5 min at frequency of 30 times/sec in the presence of TRIzol (Invitrogen), then the isolation was continued according to manufacturer's protocol. Polysomal or monosomal fractions from two experiments were pooled and mRNA was extracted using TRIzol Liquid Sample (LS) (Invitrogen) according to the manufacturer's protocol. Contaminating genomic DNA was removed using RNase-Free DNase (Qiagen) and samples were cleaned up with the RNeasy MinElute Cleanup Kit (Qiagen).

Library Preparation

RNA libraries were prepared and sequenced with the Illumina platform by Genome Scan (Leiden, Netherlands). Libraries were prepared using the NEBNext Ultra Directional RNA Library Prep Kit (NEB #E7420) according to manufacturer's protocols. Briefly, rRNA was depleted from total RNA using the rRNA depletion kit (NEB# E6310). After fragmentation of the rRNA-reduced RNA, a cDNA synthesis was performed in order to ligate with the sequencing adapters and PCR amplification of the resulting product. Quality and yields after sample preparation were measured with the Fragment Analyzer (Agilent). Sizes of the resulting products were consistent with the expected size distribution (a broad peak between 300-500 bp). Clustering and DNA sequencing using the Illumina cBot and HiSeq 4000 was performed according to manufacturer's protocol with a concentration of 3.0 nM of DNA. HiSeq control software HCS v3.4.0, image analysis, base calling, and quality check was performed with the Illumina data analysis pipeline RTA v2.7.7 and Bcl2fastq v2.17.

Read mapping, statistical analyses, and data visualization

Reads were subjected to quality control FastQC (Andrews, 2010) trimmed using Trimmomatic v0.32 (Bolger et al., 2014) and aligned to either the *C. elegans* (worm) or *M. musculus* (mouse) genomes obtained from Ensembl, wbccl235.v91 and GRCm38v87, respectively, using HISAT2 v2.0.4 (Kim et al., 2015). Worm and mouse samples were analyzed separately; different fractions (total, monosomal, polysomal) within each species were analyzed together. Counts were obtained using HTSeq (v0.6.1, default parameters) (Anders et al., 2015) using the corresponding GTF taking into account the directions of the reads. Statistical analyses were performed using the edgeR (Robinson et al., 2010) and limma/voom (Ritchie et al., 2015) R packages. All genes with more than 2 counts in at least 4 of the samples were kept. Count data were transformed to log₂-counts per million (logCPM), normalized by applying the trimmed mean of M-values method (Robinson et al., 2010) and precision weighted using voom (Law et al., 2014). All data analyses

and visualizations were done using transcript data with a count value greater than 0. Differential expression was assessed using either an empirical Bayes moderated *t*-test within limma's linear model framework including the precision weights estimated by voom (Ritchie et al 2015, Law et al 2014), or a Partial least squares discriminant analysis (PLS-DA) using mixomics (Rohart et al., 2017) setting a variable of importance (VIP) score of greater than 1 as significant. Resulting *p* values (where applicable) were corrected for multiple testing using the Benjamini-Hochberg false discovery rate. Genes were re-annotated using biomaRt using the Ensembl genome databases (v91). Data visualization was performed using gplots (Warnes et al., 2016) and ggplot2 (Wickham, 2009) selecting colors from RcolorBrewer (Neuwirth, 2014). Data processing and visualization was performed using R v3.4.3 and Bioconductor v3.5. The RNA-seq data are available on GEO under the ID GSE122097.

Translational efficiency calculations

Translational efficiencies (TEs) were acquired by considering the ratio of a highly translated ribosome-mRNA fraction (i.e. polysomal RNA) over a lower translated ribosome-mRNA fraction (i.e. either monosomal RNA for *C. elegans* or total RNA for *M. musculus*). Monosomal RNA was used for *C. elegans* as it showed an increase in abundance in our polysome profiles. The monosomal fraction did not show an increase in abundance in *M. musculus* and therefore total RNA was used. This ratio (highly translated ribosome-mRNA fraction / lower translated ribosome-mRNA fraction) was then compared between treated samples (i.e. *mrps-5* for *C. elegans* or doxycycline treatment for *M. musculus*) and control samples (i.e. empty vector for *C. elegans* or Amoxicilin treatment for *M. musculus*). This resulted in TE being defined as: $\log_2\left[\frac{\text{treated}^{\text{polysome}} / \text{treated}^{\text{monosome}}}{\text{control}^{\text{polysome}} / \text{control}^{\text{monosome}}}\right]$ in the case of *C. elegans* and $\log_2\left[\frac{\text{treated}^{\text{polysome}} / \text{treated}^{\text{total}}}{\text{control}^{\text{polysome}} / \text{control}^{\text{total}}}\right]$ in the case of *M. musculus*. Means from each set of replicates were used to calculate the ratios. A TE value was defined as significant if the gene in question had a PLS-DA VIP score above 1, in either the polysomal RNA (for both *C. elegans* and

M. musculus) or monosomal RNA (for *C. elegans*) or total RNA (for *M. musculus*), and changed at least 1.25 fold in its TE (to eliminate noise of near zero TEs).

Protein-Transcript cross comparison

Fold change (log₂ transformed) of the genes in common between the transcriptome and proteome data were plotted in a co-regulation plot, with mRNA or protein data on the X or Y axis, respectively. A cutoff was used to eliminate noise of near zero-fold change when identifying genes differentially expressed in the plot. Selecting cutoffs relative to each dataset allowed us to address the large difference in fold changes observed between the different mRNA and protein datasets, and we therefore used a quarter of the standard deviation of each log₂-transformed dataset's distribution as a standard threshold for noise (dashed line in plot). This corresponded to a value of 1.13 (0.179 in log₂ scale) for the transcriptome and 1.01 (0.016 in log₂ scale) for the proteome. Values above these cutoffs in each respective dataset that had VIP scores above 1 were considered as significant in the quadrants of the co-regulation plot.

Worm-Mouse cross comparison

Worm and mouse orthologous genes were acquired using the R package annotationTools (Kuhn et al., 2008) and HomoloGene v68 species annotation.

Ribosomal gene lists

Cytoplasmic and mitochondrial ribosomal gene lists for both *C. elegans* and *M. musculus* were downloaded from the Ribosomal Protein Gene Database (<http://ribosome.med.miyazaki-u.ac.jp/>).

Functional Annotation of gene sets

Gene sets were analysed for functional enrichments using the DAVID bioinformatics resource version 6.8 (Huang da et al., 2009). Functional annotation clustering was performed using DAVID

defined default settings incorporating gene sets from Gene Ontologies (biological process, cellular component, and molecular function), functional categories (including Clusters of Orthologous Groups (COG) ontologies, UP keywords, UP seq features), pathways (including KEGG), and protein domains (including INTERPRO PIR superfamily and SMART). Background datasets to check enrichments against included the measured transcriptome (for enrichments at mRNA level within a single species), measured proteome (for enrichments at the protein level), gene overlap between the measured transcriptome and proteome (for enrichments of the co-regulation analysis), or genes in common between mouse and worms (for cross-species enrichment). Resulting clusters were manually annotated for purposes of visualization and summarization. Clusters with an 'Enrichment Score' above 1.3 ($p < 0.05$) were considered significantly enriched.

Protein isolation for SWATH proteomics

Worm pellets were freeze-dried overnight and stored at room temperature until use. *C. elegans* proteins were isolated using the standard protocol used for tissue preparation (Wu et al., 2017) with the exception that, to ensure that the cuticle was fully ruptured, during the protein isolation from total cells in 8M urea, the samples were sonicated at a high power (150 W) for 10x10 cycles of 10 seconds (UP200St-G sonicator, Hielsher, Germany). In brief (see above source for more details): proteins were extracted in an 8M urea buffer, 300 μ g were aliquoted and precipitated by acetone overnight, then reduced with DTT, alkylated with IAA, and digested with trypsin at a 1:25 ratio. C18 spin columns (The Nest Group) were used for cleanup.

SWATH proteomics – library acquisition

For library acquisition, 150 μ g of digested peptide from three sets of pooled N2 wildtype adult *C. elegans* were pH fractionated (protocol #84868, Thermo Fisher Scientific) into 10 fractions. The resulting 30 fractions were separated on an Eksigent liquid chromatography machine coupled with a 20 cm PicoFrit emitter injected on an AbSciex 5600+ TripleTOF using a 120 minute gradient

going from 2% to 35% acetonitrile at 300 nL/minute. At the MS1 level, the 20 most intense precursors were selected in the range of 350 – 1460 m/z with a 500 ms survey scan. At the MS2 level, spectra were acquired at 150 ms survey scans between 50 - 2000 m/z. These samples were used for preparing a spectral library to support the DIA/SWATH data (Rost et al., 2014). iRT peptides (Biognosys) were added to all samples, for both DDA injections (library acquisition) and DIA injections (for quantification).

SWATH proteomics – sample acquisition

For all samples measured for quantitative DIA (SWATH) acquisition, 1 µg of non-fractionated sample were injected in the same AbSciex 5600+ TripleTOF using the same parameters except using a 60 minute gradient and in data-independent acquisition mode using 64 m/z windows. The output .wiff files from both DIA and DDA acquisition mode were converted to centroided mzXML files using FileConverter v2.2.0. For library generation from the DDA mzXML files, samples were searched against the canonical UniProtKB *C. elegans* proteome database containing 27481 proteins and searched with Comet v2016.01 r3. Reverse decoy proteins were generated and up to 2 tryptic missed cleavages were allowed with a precursor mass error of 50 ppm and fragment error of 0.1 Da. Cysteine carbamidomethylation was used as the fixed modification and methionine oxidation as the variable modification. PeptideProphet was used to search the data and scored with iProphet. A 1% protein FDR was used for significance cutoff. The in-house results from the DDA runs were combined with extensive published *C. elegans* DDA data (PXD004584) and (Narayan et al., 2016). The light channel from these SILAC-labeled samples was also searched with Comet as above, using the same parameters, using CiRT peptides instead of iRT peptides (Parker et al., 2015). The results from the in-house and downloaded DDA files were combined, and peptides with retention time variance of ≥ 150 were removed. For peptides identified in-house and in the downloaded dataset, the in-house peptide was retained and the other peptide discarded. The final assembled library contains 67'612 peptides (of which 18'072 from the in-

house DDA runs and 49'540 from the downloaded DDA runs), corresponding to 9'438 unique proteins. This library was then used as the reference library for OpenSWATH v2.1.0. OpenSWATH was run on all DIA acquisitions, followed by mProphet scoring using the msproteomicstools package available on GitHub (September 2017). 10750 peptides corresponding to 1715 proteotypic proteins were quantified. Protein data were generated from the peptide matrix using MSstats v3.12.0. Differential expression was determined using either a Student's *t*-test (with *p* values corrected for multiple testing using the Benjamini-Hochberg false discovery rate, presented for reference) or partial least squares discriminant analysis (PLS-DA) with mixomics (Rohart et al., 2017) setting a variable of importance (VIP) score of greater than 1 as significant. The DIA data and the assembled library file are available on PRIDE under the ID PXD009223. *Reviewer access is available under the login: reviewer91362@ebi.ac.uk and password: vrOYX09z.*

QUANTIFICATION AND STATISTICAL ANALYSIS

Statistical details and tests used, the number and representation of *n* and any other forms of quantification present are specified in the respective figure legends and results section. Statistical analyses for quantified polysome profiles and western blotting (WB) were performed using the Prism 7 software (GraphPad Software, La Jolla, CA, USA). Significance was tested with Student's *t*-test, and *p* values were adjusted to correct for multiple testing using the Holm-Šídák method. All other statistics were performed as described in each respective methods section and unless otherwise noted, were performed using R v3.4.3. Gene expression was considered differential relative to control using the variable of importance (VIP) score from a partial least squares discriminant analysis (PLSA-DA) greater than 1. In all supplemental tables where relevant, *p* values (Bayes moderated *t*-test for transcriptomics or Student's *t*-test for proteomics), and adjusted *p* values (Benjamini-Hochberg method) are presented in addition to the VIP scores (from PLS-DA).

DATA AND SOFTWARE AVAILABILITY

The accession number for the *C. elegans* and mice RNA sequencing data reported in this paper is GEO: GSE122097. The proteomics DIA data and the assembled library file are available on PRIDE under the ID PXD009223. The reference liver mouse transcriptomics and proteomics data examined in Figure 1 are available under GEO at GSE60149 and PRIDE at PXD003266. The reference multi-tissue mouse transcriptome data are available under GEO GSE60149, GSE60150, GSE60151, and GSE60489 and are from the same mice despite the non-continuous and separate entries. The multi-tissue proteomics data are from PXD005044. Note that the raw liver proteomics data from PXD003266 from 2016 were re-analyzed using the newer SWATH search library from PXD005044 from 2018, which was designed to improve coverage for mitochondrial proteins. These re-processed and normalized and processed mouse data are also available as Supplemental Table S1.

Supplemental tables

Table S1. Re-analyzed liver proteomics data from PXD003266, related to Figure 1

Table S2. Monosomal/polysomal RNA-seq and translational efficiency worm, related to Figure 2.

Table S3. Total RNA-seq worm, Related to Figure 3

Table S4. Proteome worm, Related to Figure 3

Table S5. Proteome transcriptome coregulation worm, Related to Figure 3 and table S3-4

Table S6. RNA-seq mice, Related to Figure 5

Table S7. Cross species RNA-seq comparison, Related to Figure 5

Figure 1

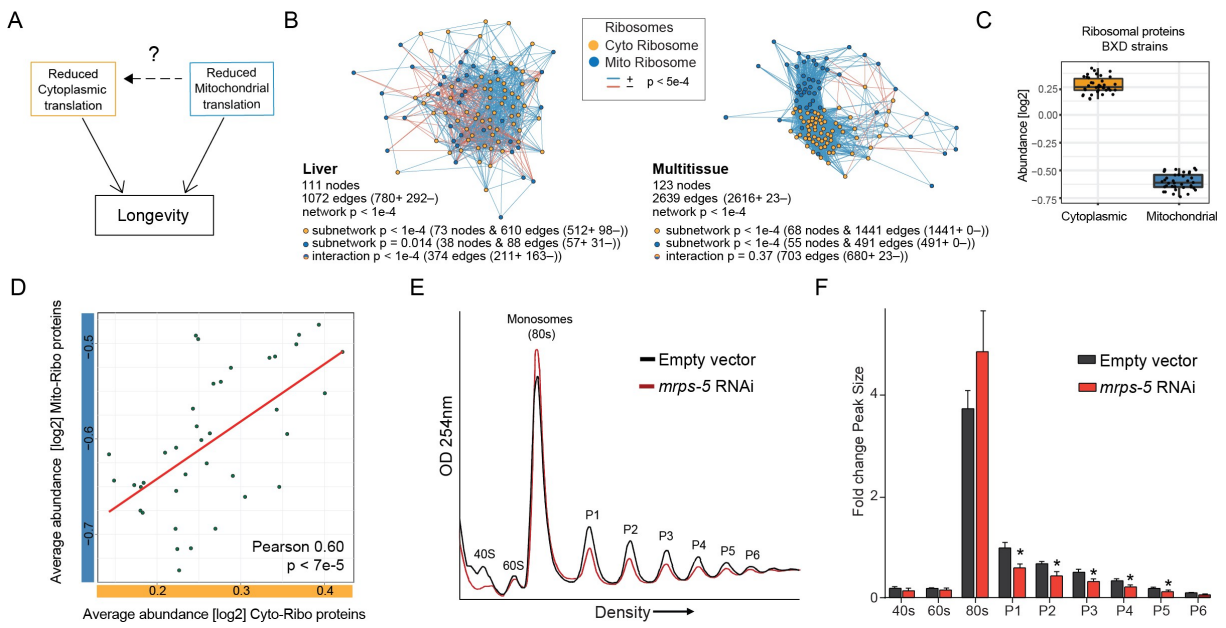


Figure 2

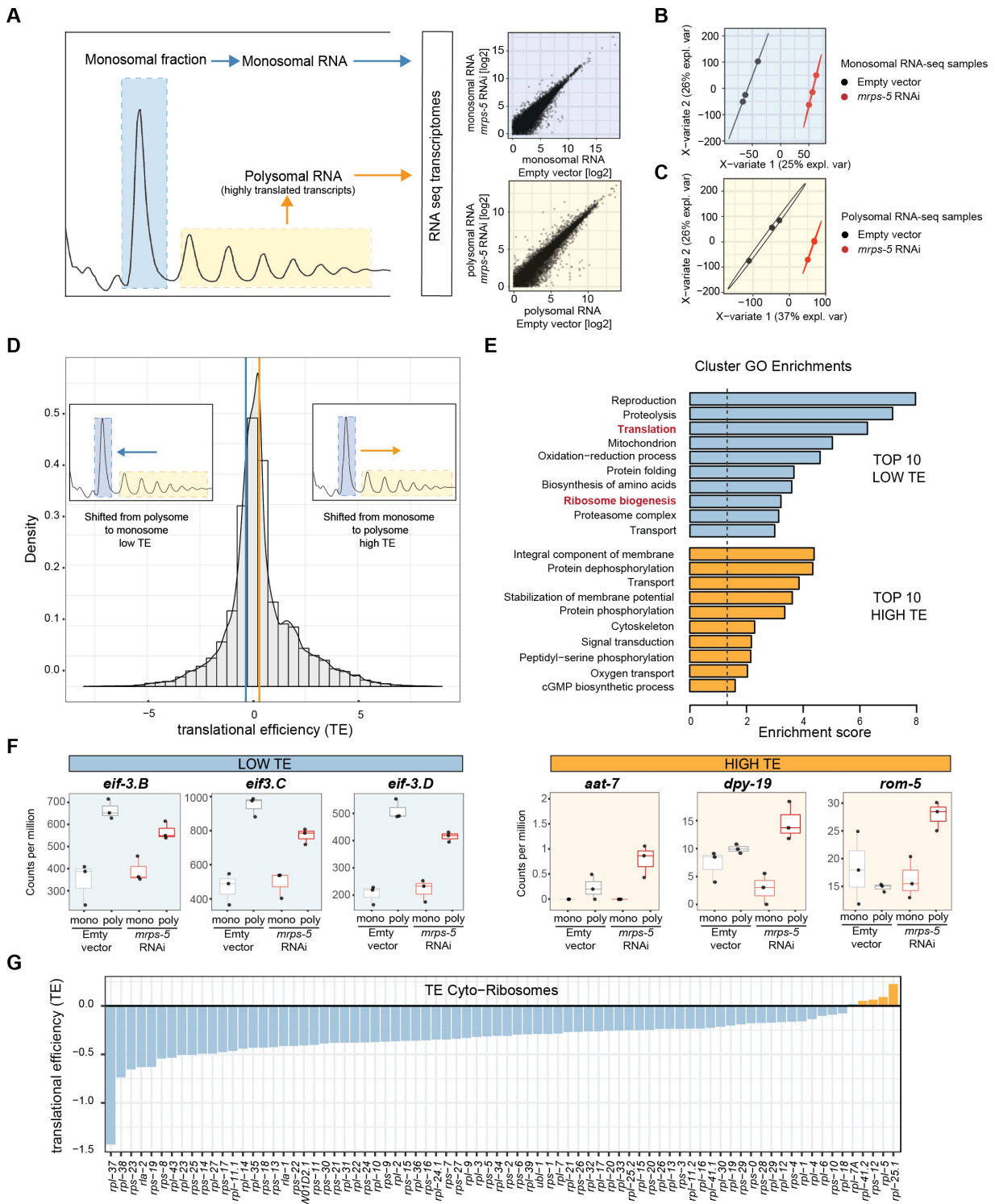


Figure 3

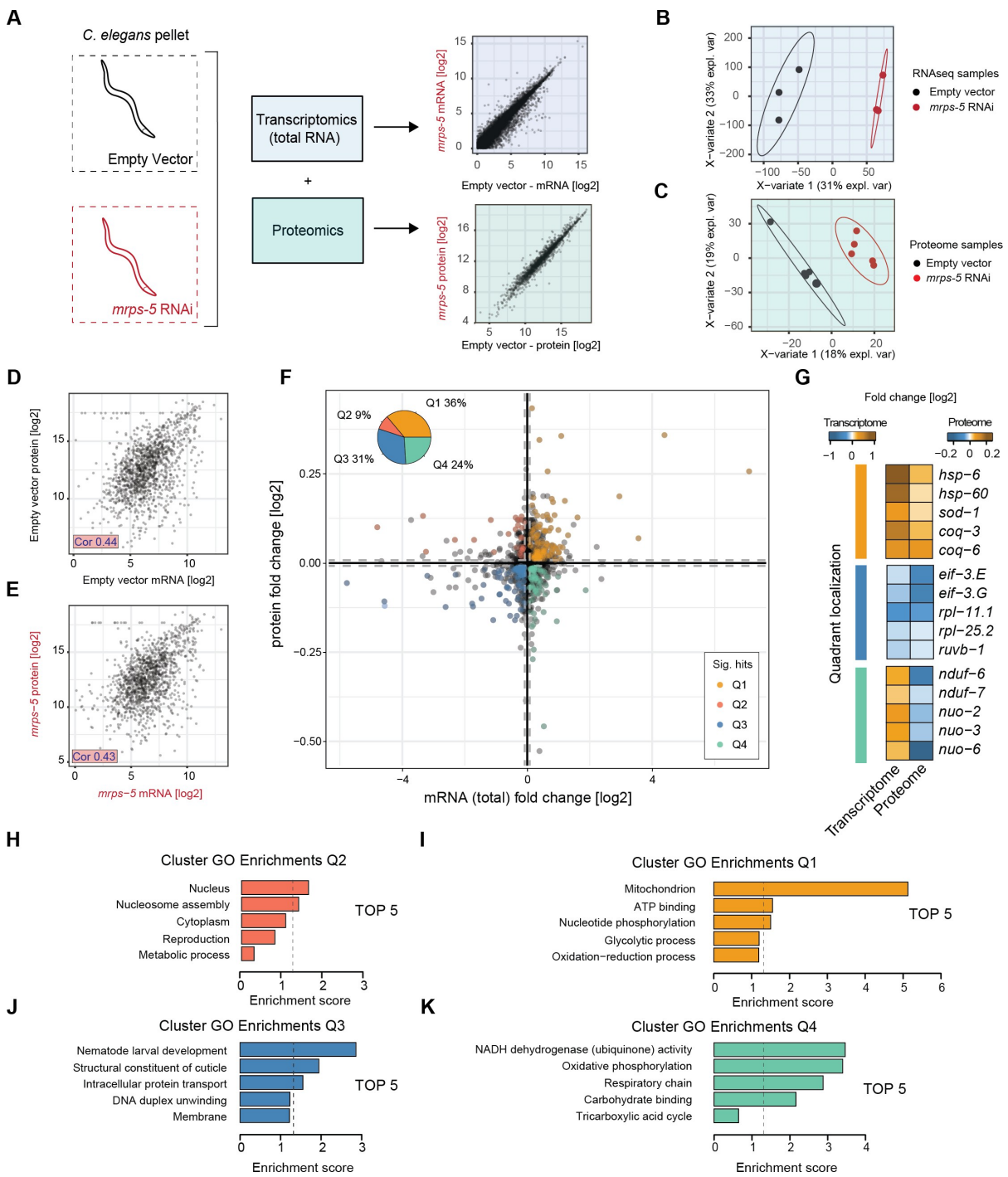


Figure 4

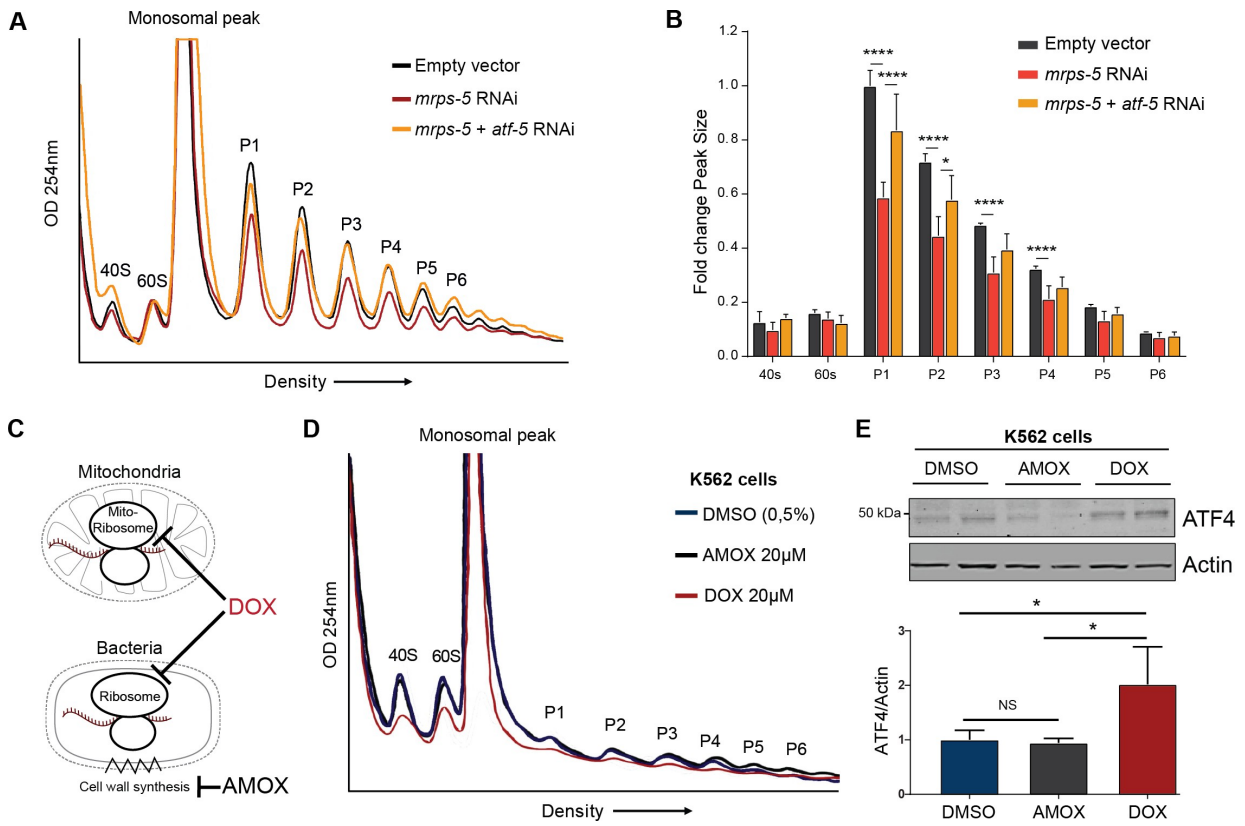
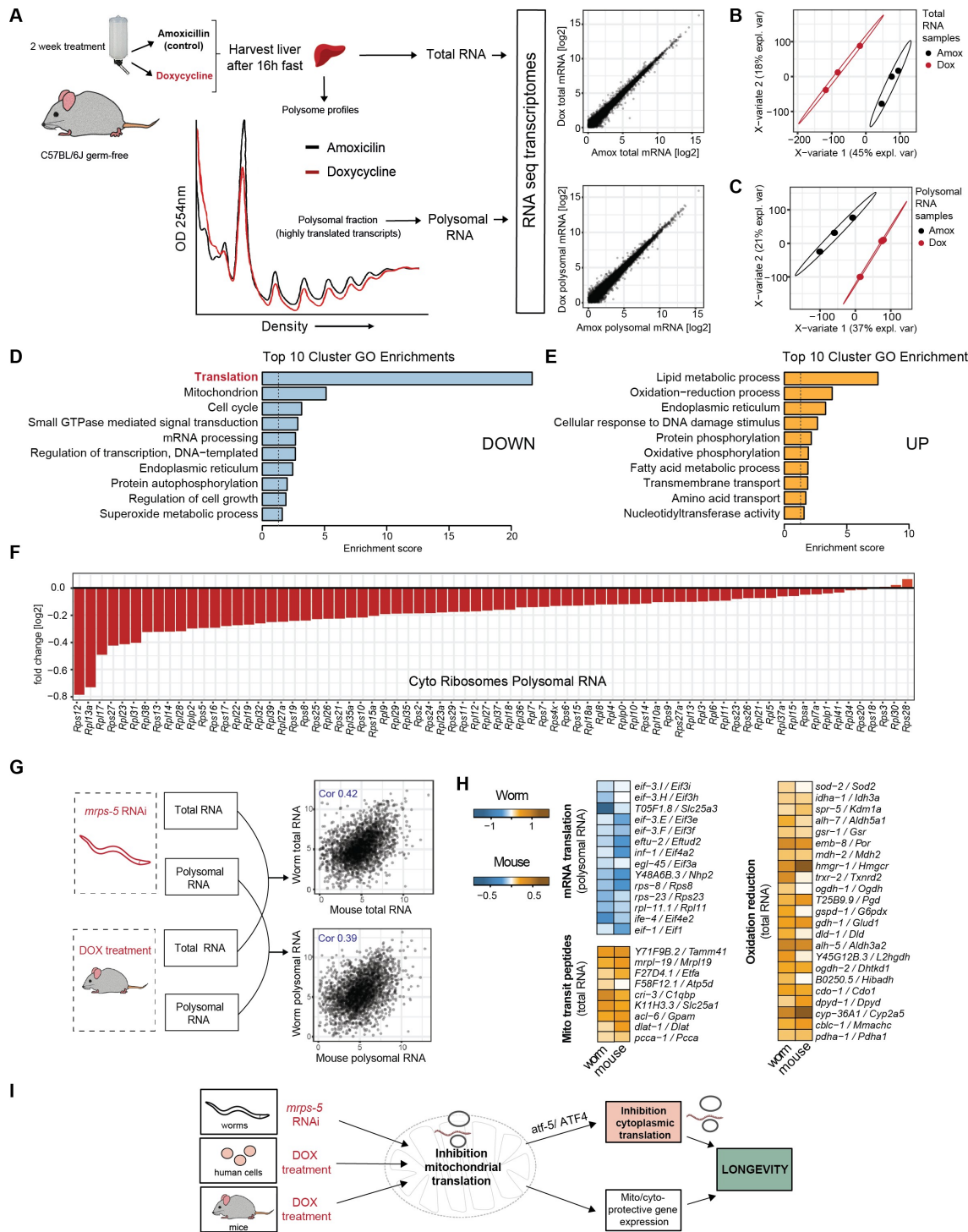


Figure 5



Key resources

REAGENT or RESOURCE	SOURCE	IDENTIFIER
Antibodies		
Rabbit monoclonal anti-ATF4	Cell Signaling Technology	Cat# 11815 RRID: AB_2616025
Mouse monoclonal anti- β -Actin	Sigma-Aldrich	Cat# A5441 RRID: AB_476744
Donkey anti-Rabbit IgG	LI-COR Biosciences	Cat# 925-68073 RRID: AB_2716687
Goat anti-mouse IgG	LI-COR Biosciences	Cat# 925-32210 RRID: AB_2687825
Bacterial and Virus Strains		
<i>Escherichia coli</i> : OP50	Caenorhabditis Genetics Center	RRID:WB-STRAIN:OP50
<i>Escherichia coli</i> : HT115 (DE3)	Caenorhabditis Genetics Center	RRID:WB-STRAIN:HT115(DE3)
Ahringer <i>C. elegans</i> RNAi library	Source BioScience	http://www.sourcebioscience.com/products/life-science-research/clones/rnai-resources/c-elegans-rnai-collection-ahringier/
Biological Samples		
Chemicals, Peptides, and Recombinant Proteins		
Cycloheximide	Sigma	Cat# C6255
Doxycycline	Sigma	Cat# D9891
Amoxicillin	Sigma	Cat# A8523
DMSO	Sigma	Cat# D8418
Critical Commercial Assays		
BCA protein assay Reagent A	Thermo Fisher Scientific	#23223
TRIzol (LS)	Invitrogen	#15596026 (#10296010)
RNeasy MinElute Cleanup Kit	Qiagen	#74204
NEBNext Ultra Directional RNA Library Prep Kit	NEB	#E7420
rRNA depletion kit	NEB	# E6310
Deposited Data		
<i>C. elegans</i> and Mouse RNA-seq data	This paper	GEO: GSE122097
<i>C. elegans</i> Proteomics data	This paper	PRIDE: PXD009223
BXD mouse liver proteome data (reprocessed)	This paper	Table S1
BXD mouse liver proteome data	Genenetwork.org	GN540
BXD mouse multi tissue proteome data	Molecular and Cellular Proteomics Journal	DOI: 10.1074/mcp.RA118.000554
Experimental Models: Cell Lines		
Human: K562 cells	ATCC	CCL-243 RRID:CVCL_0004
Experimental Models: Organisms/Strains		

<i>C. elegans</i> : N2 Bristol	Caenorhabditis Genetics Center (CGC); http://cbs.umn.edu/cgc/home	CGC:10570 RRID:WB-STRAIN: N2_(ancestral)
Mouse: C57BL/6J germ-free	INRA Research Center	
Oligonucleotides		
Recombinant DNA		
Software and Algorithms		
R (v3.4.3)	https://www.r-project.org	v3.4.3
FastQC	(Andrews, 2010) https://www.bioinformatics.babraham.ac.uk/projects/fastqc/	NA
iGraph v1.2.1 package	https://CRAN.R-project.org/package=igraph	v1.2.1
RTA v2.7.7	Illumina.com, Real-Time Analysis	V2.7.7
Bcl2fastq v2.17	Illumina.com	V2.17
Trimmomatic v0.32	(Bolger et al., 2014) http://www.usadellab.org/	v0.32
HISAT2 v2.0.4	(Kim et al., 2015) https://ccb.jhu.edu/software/hisat2/index.shtml	v2.0.4
HTSeq v0.6.1	(Anders et al., 2015) https://htseq.readthedocs.io/en/release_0.10.0/	v0.6.1
Comet v2016.01 r3	doi: 10.1002/pmic.201200439	v2016.01 r3
OpenSWATH v2.1.0	http://www.openswath.org/	v2.1.0
MSstats v3.12.0	http://msstats.org/	v3.12.0
Limma/voom	(Ritchie et al., 2015)/(Law et al., 2014) https://bioconductor.org/packages/release/bioc/html/limma.html	NA
edgeR	(Robinson et al., 2010) https://bioconductor.org/packages/release/bioc/html/edgeR.html	NA
HiSeq control software HCS v3.4.0	https://support.illumina.com/downloads/hiseq-x-hcs-v3-4-0.html	v3.4.0
Bioconductor v3.5	https://www.bioconductor.org/install/	v3.5
GraphPad Prism v7.03	GraphPad Software, Inc. https://www.graphpad.com/scientific-software/prism/	v7.03
ImageJ	National Institutes of Health https://imagej.nih.gov/ij/	NA
Other		

Supplemental Information

A conserved mito-cytoplasmic translational balance links two longevity pathways

Marte Molenaars, Georges E. Janssens, Evan G. Williams, Aldo Jongejan, Jiayi Lan, Sylvie Rabot, Fatima Joly, Perry D. Moerland, Antoine H.C. van Kampen, Ruedi Aebersold, Alyson W. MacInnes, Riekelt H. Houtkooper

Figure S1

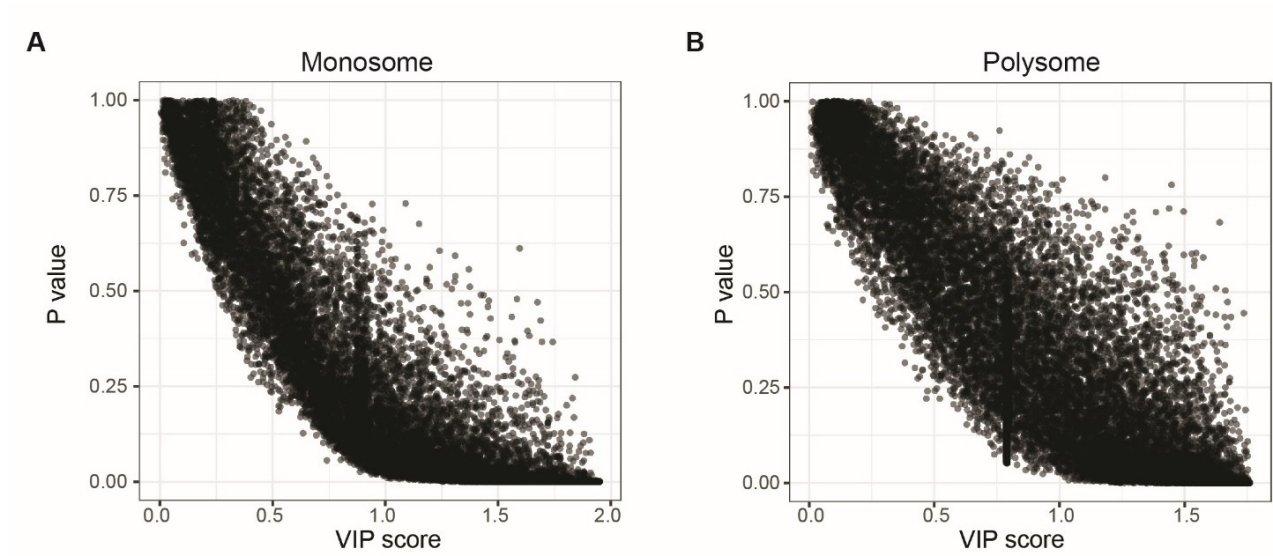


Figure S1. VIP score correlates highly to traditional p -value ranking, related to Figure 2 and Table S2.

(A-B) Partial least squares discriminant analysis (PLS-DA) derived a variable of importance (VIP) score for each gene. Bayes moderated t -test used to derive p values. Performed for both (A) monosomal and (B) polysomal RNAseq results.

Figure S2

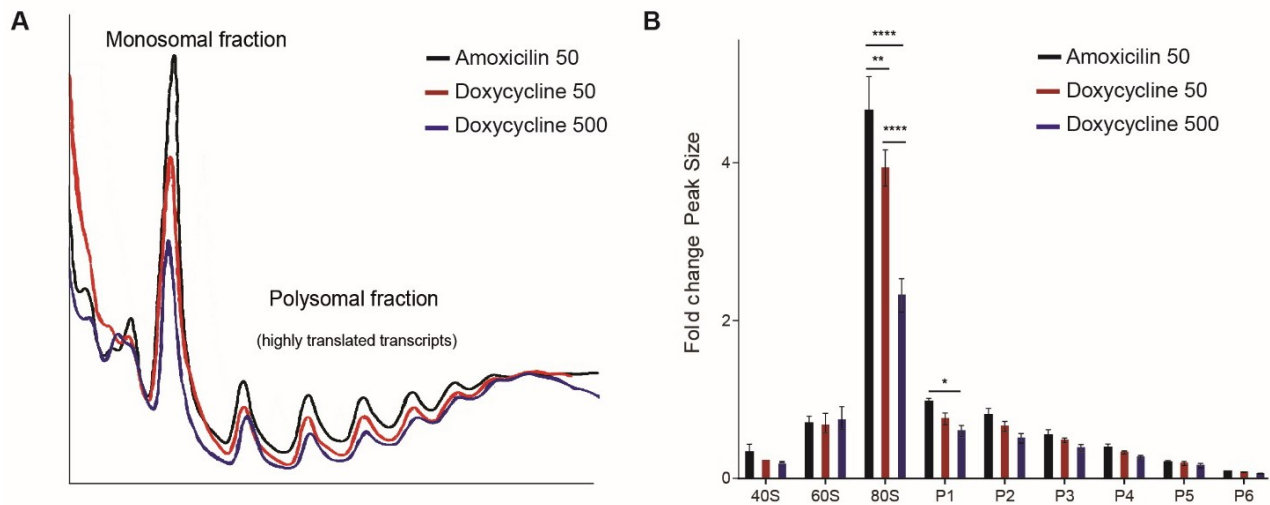


Figure S2. Doxycycline treatment resulted in suppression of global translation in liver in a dose-dependent manner, related to Figure 5.

(A) Representative polysome profiles showing decreased cytoplasmic polysome abundances in the liver of mice treated with either a low dose of doxycycline (50 mg/kg/d) or a high dose of doxycycline (500 mg/kg/d) compared to control amoxicillin-treated mice (50 mg/kg/d). Lysate is normalized to protein levels.

(B) Quantification of polysome peak sizes with N=3 mice per condition normalized to P1 peak of amoxicillin-treated mice. Bars represent mean \pm SEM and significance was tested with Student's t-test, and p -values were adjusted to correct for multiple testing using the Holm-Šídák method, with $\alpha = 0.05$.

Figure S3

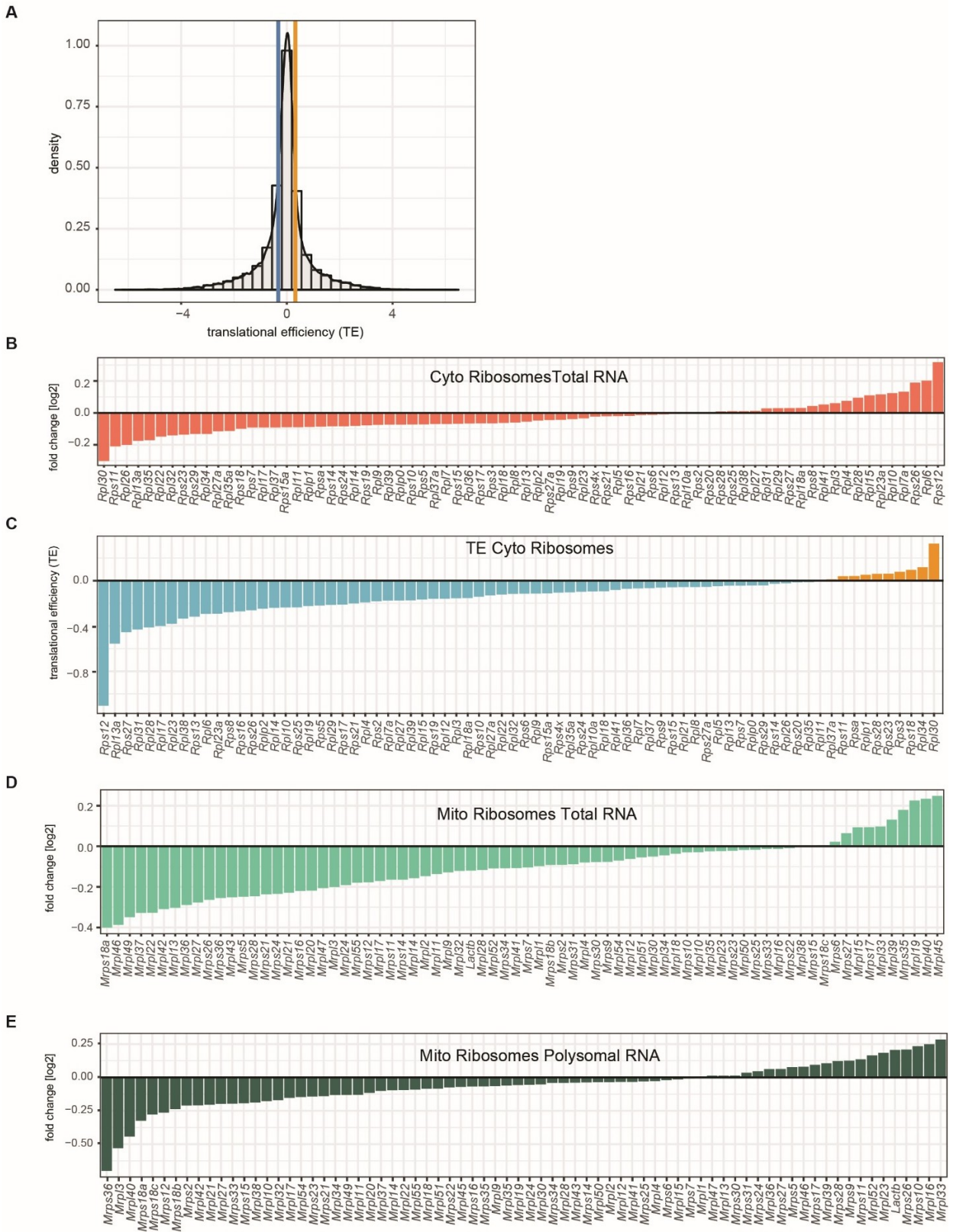


Figure S3. Translational efficiency (TE) plot and expression of individual cytoplasmic and mitochondrial ribosomal proteins in doxycycline-treated mouse livers, Related to figure 5 and Table S6.

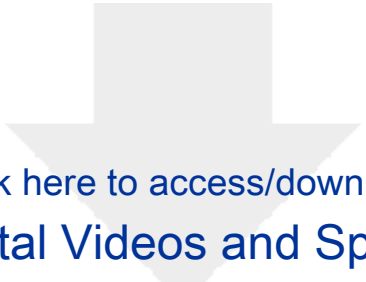
(A) Translational efficiencies (TE) of transcripts, defined as the log₂ ratio of polysomal vs total differences between doxycycline-treated mice (50 mg/kg/d) and control amoxicillin-treated mice (50 mg/kg/d) gene expression, shows shifts in transcripts from either the monosome to the polysome (high TE, yellow) or the polysome to the monosome (low TE, blue).

(B) Fold changes of individual cytoplasmic ribosomal proteins in the total RNA in doxycycline-treated mouse livers.

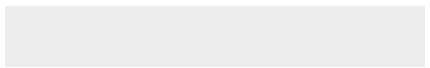
(C) Individual cytoplasmic ribosomal proteins have a low TE in doxycycline-treated mice (50 mg/kg/d) compared to control amoxicillin-treated mice. TE of transcripts defined as the log₂ ratio of polysomal vs monosomal differences between doxycycline-treated (50 mg/kg/d) and amoxicillin-treated mice gene expression.

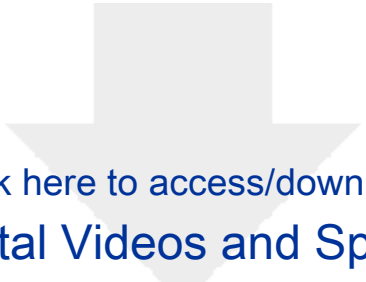
(D) Fold changes of individual mitochondrial ribosomal proteins in the total RNA in doxycycline-treated mouse livers.

(E) Fold changes of individual mitochondrial ribosomal proteins in the polysomal RNA in doxycycline-treated mouse livers.

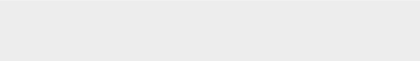


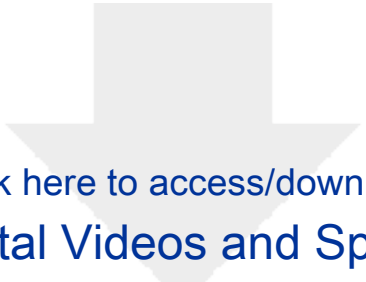
[Click here to access/download](#)
Supplemental Videos and Spreadsheets
Table S1.xlsx



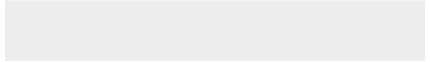


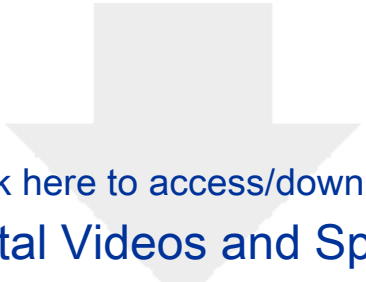
[Click here to access/download](#)
Supplemental Videos and Spreadsheets
Table S2.xlsx



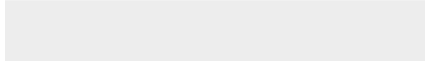


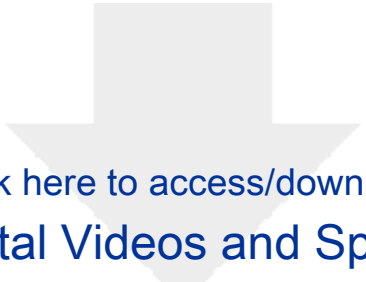
[Click here to access/download](#)
Supplemental Videos and Spreadsheets
Table S3.xlsx



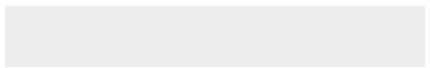
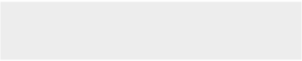


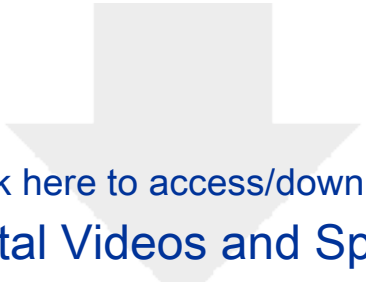
[Click here to access/download](#)
Supplemental Videos and Spreadsheets
Table S4.xlsx



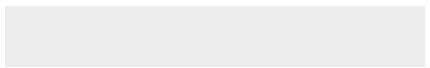


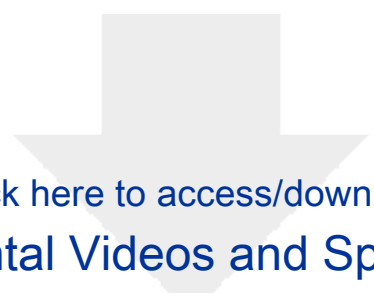
[Click here to access/download](#)
Supplemental Videos and Spreadsheets
Table S5.xlsx





[Click here to access/download](#)
Supplemental Videos and Spreadsheets
Table S6.xlsx





[Click here to access/download](#)
Supplemental Videos and Spreadsheets
Table S7.xlsx

